the Human Genome Variation Society (http://www.hgvs.org/mutnomen).

In addition, all exons and adjacent intronic regions of the *PRSS1*, *SPINK1*, *CTRC*, and *CPA1* genes were amplified by PCR and directly sequenced as previously reported [5, 6, 8, 25].

In Silico Prediction

SIFT (Sorting Intolerant From Tolerant; http://sift.jcvi.org/) and PolyPhen-2 (http://genetics.bwh.harvard.edu/pph2/) were used to predict whether an amino acid substitution would affect the structure and function of a protein. SIFT uses sequence homology, whereas PolyPhen-2 offers predictions based on conservation, protein folding, and crystal structure [26, 27]. The SIFT scores range from zero to one, with zero predicted to be the most deleterious mutation and one the least deleterious. The PolyPhen-2 scoring predicts three outcomes for mutations: "benign" (most likely lacking any phenotypic effect), "possibly damaging" (may affect protein structure or function), and "probably damaging" (high degree of confidence that protein structure function will be affected).

Statistical Analysis

The variant frequencies in the Japanese population were obtained from the Human Genetic Variation Database (www.genome.med.kyoto-u.ac.jp/SnpDB/). The significance of the differences in variant frequencies between patients and controls was tested by two-tailed Fisher's exact test. A P value <0.05 was considered significant. All statistical analyses were performed using the SPSS version 17.0 statistical analysis software (SPSS Inc., Chicago, IL, USA).

Results

Approximately 10 kb of the coding regions and the adjacent noncoding regions of the *CFTR* gene were analyzed in this study. On average, 98.8, 97.0, and 95.1 % of the coding regions of the *CFTR* gene were covered by at least one, five, and 10 sequence reads, respectively. The sequencing data covered 91.6 % of the coding regions of the *CFTR* gene by ≥20 reads with a mean read depth of 449 and a median depth of 412 (Fig. 1). These results indicate a high-resolution capability for the identification of variants, such as mutations.

In our cohort of 193 CP patients, we identified 12 non-synonymous and seven synonymous variants in the exons of the *CFTR* gene by targeted NGS (Tables 2, 3, 4, 5). The presence of these variants was confirmed by Sanger sequencing. Based on the presence in dbSNP137, Exome Variant Server (NHLBI GO Exome Sequencing Project, Seattle, WA, USA; URL: http://evs.gs.washington.edu/EVS/), and the Human Genetic Variation Database, three non-synonymous variants [c.1231A>G (p.K411E), c.1753G>T (p.E585X) and c.2869delC (p.L957fs)] and three synonymous variants (c.372C>T, c.3975A>G and c.4254G>A) were novel. The frameshift variant c.2869delC (p.L957fs) leads to a stop codon afterward at amino acid 967, to premature termination of translation and a heavily truncated protein missing more than one-third of its amino acids. This variant was found in a 22-year-old female with idiopathic CP. She was admitted due to a pancreatitis attack and diagnosed as having CP. She had suffered from back and abdominal pain since 20 years old. The value of the *n*-benzoyl-*l*-tyrosyl-*p*-aminobenzoic acid test was 52 % (normal: >70 %), suggesting pancreatic exocrine dysfunction. The patient also had the c.4056G>C (p.Q1352H) variant in a

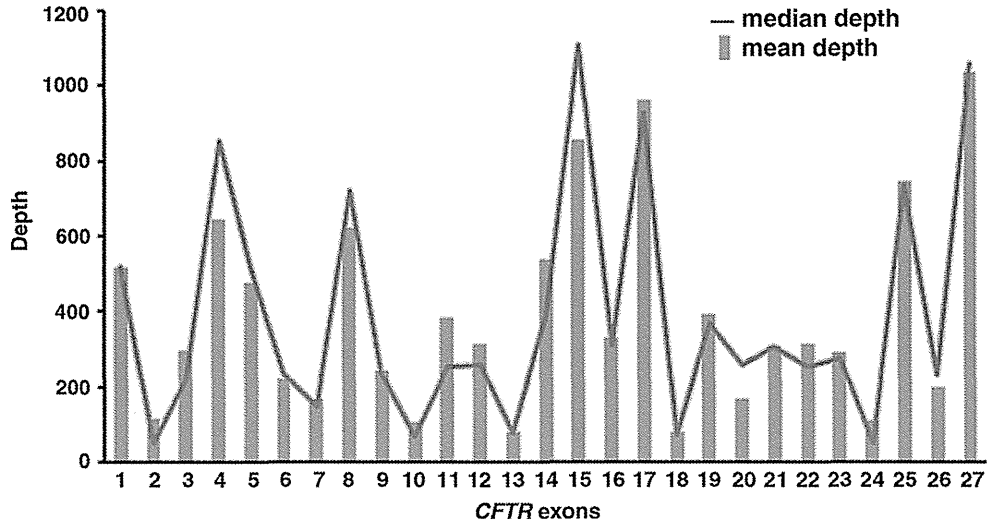

Fig. 1 Graph of the mean depth, median depth, and sequencing coverage for all the 27 exons in the *CFTR* gene. By MiSeq NGS, a high-quality sequence was obtained for 27 exons and the flanking sequences from the *CFTR* gene, including a mean depth of ×516 and a median depth of ×442. On average, 90.3 % of the coding region was successfully covered by ≥20 reads

Table 2 Non-synonymous *CFTR* variants detected in this study

Exon	Non-synonymous variant	Amino acid change	dbSNP135	Genotype	SIFT (score)	PolyPhen-2 (score)	Alcoholic CP (%)	Idiopathic CP (%)	Hereditary/ familial CP (%)
2	c.91C>T	p.R31C	rs1800073	CT	D (0.012)	PD (0.989)	0/46 (0)	3/121 (2.5)	0/26 (0)
2	c.92G>A	p.R31H	rs149353983	GA	T (0.183)	B (0.003)	0/46 (0)	1/121 (0.8)	0/26 (0)
4	c.374T>C	p.I125T	rs141723617	TC	D (0.005)	B (0.17)	0/46 (0)	2/121 (1.6)	1/26 (3.8)
10	c.1231A>G	p.K411E	–	AG	D (0.015)	B (0.233)	0/46 (0)	1/121 (0.8)	0/26 (0)
11	c.1408G>A	p.V470M	rs213950	GA	T (1)	B (0)	21/46 (45.7)	65/121 (53.7)	11/26 (42.3)
				AA			5/46 (10.9)	19/121 (15.7)	1/26 (3.8)
12	c.1666A>G	p.I556V	rs75789129	AG	T (0.536)	B (0.334)	2/46 (4.3)	8/121 (6.6)	0/26 (0)
				GG			0/46 (0)	0/121 (0)	0/26 (0)
13	c.1753G>T	p.E585X	–	GT	–	–	1/46 (2.2)	0/121 (0)	0/26 (0)
17	c.2869delC	p.L957fs	–		–	–	0/46 (0)	1/121 (0.8)	0/26 (0)
21	c.3468G>T	p.L1156F	rs139729994	GT	T (0.163)	PD (0.994)	2/46 (4.3)	10/121 (8.3)	2/26 (7.7)
				TT			1/46 (2.2)	0/121 (0)	0/26 (0)
25	c.4045G>A	p.G1349S	rs201686600	GA	D (0)	PD (1)	1/46 (2.2)	0/121 (0)	0/26 (0)
25	c.4056G>C	p.Q1352H	rs113857788	GC	D (0)	PD (1)	5/46 (10.9)	11/121 (9.1)	4/26 (15.4)
				CC			0/46 (0)	0/121 (0)	0/26 (0)
27	c.4357C>T	p.R1453W	rs4148725	CT	D (0)	PD (0.999)	3/46 (6.5)	6/121 (5.0)	1/26 (3.8)

B benign, *CP* chronic pancreatitis, *D* damaging, *PD* probably damaging, *T* tolerated, *SIFT* Sorting Intolerant From Tolerant

Table 3 Comparison of the non-synonymous variant frequencies between the patients with CP and controls

Amino acid change	Genotype	All CP (%)	HGVD (%)	*P* value (vs. HGVD)				
				All CP	Alcoholic CP	Nonalcoholic CP	Idiopathic CP	Hereditary/ familial CP
p.R31C	CT	3/193 (1.6)	12/1102 (1.1)	0.48	>0.99	0.41	0.18	>0.99
p.R31H	GA	1/193 (0.5)	0	–	–	–	–	–
p.I125T	TC	3/193 (1.6)	5/1102 (0.5)	0.11	>0.99	0.057	0.15	0.13
p.K411E	AG	1/193 (0.5)	0	–	–	–	–	–
p.V470M	GA	97/193 (50.3)	573/1199 (47.8)	0.66	0.57	0.68	0.38	0.12
	AA	25/193 (13.0)	185/1199 (15.4)					
p.I556V	AG	10/193 (5.2)	78/1150 (6.8)	0.70	0.79	0.81	>0.99	0.45
	GG	0/193 (0)	3/1150 (0.3)					
p.E585X	GT	1/193 (0.5)	0	–	–	–	–	–
p.L957fs		1/193 (0.5)	0	–	–	–	–	–
p.L1156F	GT	14/193 (7.3)	45/1136 (4.0)	0.04	0.06	0.07	0.11	0.30
	TT	1/193 (0.5)	1/1136 (0.1)					
p.G1349S	GA	1/193 (0.5)	4/1094 (0.4)	0.56	0.19	>0.99	>0.99	>0.99
p.Q1352H	GC	20/193 (10.4)	57/1153 (4.9)	0.009	0.12	0.037	0.17	0.062
	CC	0/193 (0)	1/1153 (0.1)					
p.R1453W	CT	10/193 (5.2)	42/1144 (3.7)	0.32	0.25	0.49	0.45	>0.99

CP chronic pancreatitis, *HGVB* Human Genetic Variation Database

P values were determined versus HGVD by the Fisher's exact test

Table 4 Synonymous variants in the exons of the *CFTR* gene detected in this study

Exon	Synonymous variant	Amino acid change	dbSNP135	Genotype	Alcoholic CP (%)	Idiopathic CP (%)	Hereditary/ familial CP (%)
4	c.372C>T	p.G124=	–	CT	0/46 (0)	1/121 (0.8)	0/26 (0)
13	c.1731C>T	p.Y577=	rs55928397	CT	0/46 (0)	1/121 (0.8)	0/26 (0)
15	c.2562T>G	p.T854=	rs1042077	TG	20/46 (43.5)	69/121 (57.0)	12/26 (46.2)
				GG	6/46 (13.0)	18/121 (14.9)	0/26 (0)
23	c.3723C>A	p.G1241=	rs185065886	CA	1/46 (2.2)	0/121 (0)	0/26 (0)
25	c.3975A>G	p.R1325=	–	AG	0/46 (0)	1/121 (0.8)	0/26 (0)
27	c.4254G>A	p.E1418=	–	GA	0/46 (0)	1/121 (0.8)	0/26 (0)
27	c.4389G>A	p.Q1463=	rs1800136	GA	1/46 (2.2)	3/121 (2.5)	0/26 (0)

CP chronic pancreatitis

heterozygous form (Table 6). The nonsense variant c.1753G>T (p.E585X) was found in a patient with alcoholic CP. He was diagnosed as having alcoholic CP at 28 years old. The c.1231A>G (p.411E) variant was found in a 19-year-old male with idiopathic CP. He had suffered from pancreatitis attacks since 12 years old. ERCP showed multiple stones in the main pancreatic duct. He underwent extracorporeal shock wave lithotripsy for the treatment of pancreatic stones. The patient also had the c.3468G>T (p.L1156F) variant in a heterozygous form. None of these three patients had known pancreatitis susceptibility mutations in the *PRSS1*, *SPINK1*, *CTRC*, or *CPA1* genes (Table 6). All of the patients carrying the novel synonymous variants were idiopathic CP (Table 4).

The frequency of the c.4056G>C (p.Q1352H) variant was higher in all patients with CP than that in controls ($P = 0.009$; Table 3). Stratification based on the etiologies showed that the association was significant in patients with nonalcoholic CP (combination of cases with idiopathic, hereditary, and familial CP) ($P = 0.037$). The frequency of the c.3468G>T (p.L1156F) variant was also higher in patients with CP than that in controls ($P = 0.04$). There were no significant difference for any other non-synonymous or synonymous variants detected in the exons

Table 5 Comparison of the synonymous variant frequencies between the patients with CP and controls

Synonymous variant	Genotype	All CP (%)	HGVD (%)	*P* value (vs. HGVD)				
				All CP	Alcoholic CP	Nonalcoholic CP	Idiopathic CP	Hereditary/ familial CP
c.C372T	CT	1/193 (0.5)	0	–	–	–	–	–
c.1731C>T	CT	1/193 (0.5)	0	–	–	–	–	–
c.2562T>G	TG	101/193 (52.3)	528/1154 (45.8)	0.22	0.81	0.11	0.045	0.033
	GG	24/193 (12.4)	181/1154 (15.7)					
c.3723C>A	CA	1/193 (0.5)	3/671 (4.5)	>0.99	0.23	>0.99	>0.99	>0.99
c.3975A>G	AG	1/193 (0.5)	0	–	–	–	–	–
c.4254G>A	GA	1/193 (0.5)	0	–	–	–	–	–
c.4389G>A	GA	4/193 (2.1)	40/1112 (3.6)	0.48	>0.99	0.53	0.81	>0.99
	AA	0/193 (0)	1/1112 (0.1)					

CP chronic pancreatitis, *HGVD* Human Genetic Variation Database

P values were determined against HGVD by the Fisher's exact test

Table 6 Total *CFTR* sequencing results of patients carrying rare non-synonymous *CFTR* variants

Case#	Etiology	Age at onset	Rare variant	Additional non-synonymous variants	c.1210-34TG(9_13) c.1210-12T(5_9)	Mutation in other pancreatitis susceptibility genes[a]
A1	Idiopathic	34	p.R31C/-	p.R1453W/-	TG11/TG11, 7T/7T	–
A2	Idiopathic	8	p.R31C/-	–	TG11/TG12, 7T/7T	–
A3	Idiopathic	16	p.R31C/-	–	TG11/TG12, 7T/7T	–
A4	Idiopathic	10	p.R31H/-	–	TG11/TG12, 7T/7T	–
A5	Idiopathic	16	p.I125T/-	p.L1156F/-	TG11/TG12, 7T/7T	*CTRC* p.R29Q/-
A6	Idiopathic	2	p.I125T/-	–	TG11/TG12, 7T/7T	–
A7	Hereditary	28	p.I125T/-	p.R1453W/-	TG11/TG12, 7T/7T	–
A8	Idiopathic	19	p.K411E/-	p/L1156F/-	TG11/TG12, 7T/7T	–
A9	Alcoholic	28	p.E585X/-	p.I556V/-	TG11/TG11, 7T/7T	–
A10	Idiopathic	21	p.L957fs/-	p.Q1352H/-	TG11/TG12, 7T/7T	–
A11	Alcoholic	40	p.G1349S/-	–	TG11/TG11, 7T/7T	–

[a] Pancreatitis-associated mutations in the *PRSS1*, *SPINK1*, *CTRC*, and *CPA1* genes

between all patients with CP and controls (Tables 3, 5). The frequency of the c.2562T>G variant was different between the controls and the patients with idiopathic or hereditary/familial CP.

The 5T and, more rarely, 3T splicing variants of the intron 9 acceptor splice site [c.1210-12T(5_9)] are considered to be variants associated with CFTR-RD [16]. The 5T or 3T allele is a polymorphic variant with variable penetrance, causing less efficient exon 10 splicing and a lower *CFTR* transcript level [28]. The splicing efficiency of exon 10 is further affected by the length of the adjacent TG repeat [c.1210-34TG(9_13)]. The distribution of the c.1210-34TG(9_13) and c.1210-12T(5_9) variants is shown in Table 7. In our cohort, nine patients with CP had the 5T allele, all in a heterozygous form. Four patients (two alcoholic, one idiopathic, one hereditary) had the 5T-TG13. No patient had the haplotype TG10-7T-M470, which was reported to increase the risk of idiopathic CP [28].

It has been increasingly recognized that compound and trans-heterozygosity in the pancreatitis susceptibility genes are an overt risk factor for idiopathic CP [29–32]. Among the 193 patients with CP enrolled in this study, 29 patients had pancreatitis-associated mutations in the *PRSS1*, *SPINK1*, *CTRC*, and *CPA1* genes. Among these, nine patients had the non-synonymous *CFTR* variants, which are probably damaging based on the SIFT and/or the PolyPhen-2 prediction (Table 8).

Discussion

In this study, we performed comprehensive analysis of the variants in the *CFTR* gene by targeted NGS. To our knowledge, this is the first study to analyze pancreatitis susceptibility genes by targeted NGS. Comprehensive analysis by targeted NGS enabled us to identify novel and

Table 7 Distribution of the c.1210-34TG(9_13) and c.1210-12T(5_9) variants in patients with CP

c.1210-34TG(9_13), c.1210-12T(5_9)	All CP (%)	Alcoholic CP (%)	Idiopathic CP (%)	Hereditary/ familial CP (%)
TG10/TG11, 7T/9T	1/193 (0.5)	0/46 (0)	1/121 (0.8)	0/26 (0)
TG11/TG11, 7T/7T	46/193 (23.8)	15/46 (32.6)	23/121 (19.0)	8/26 (30.8)
TG11/TG11, 7T/9T	4/193 (2.1)	1/46 (2.2)	3/121 (2.5)	0/26 (0)
TG11/TG12, 5T/7T	5/193 (2.6)	0/46 (0)	4/121 (3.3)	1/26 (3.8)
TG11/TG12, 6T/7T	1/193 (0.5)	0/46 (0)	1/121 (0.8)	0/26 (0)
TG11/TG12, 7T/7T	124/193 (64.2)	27/46 (58.7)	81/121 (66.9)	16/26 (61.5)
TG11/TG13, 6T/7T	1/193 (0.5)	1/46 (2.2)	0/121 (0)	0/26 (0)
TG11/TG13, 7T/7T	1/193 (0.5)	0/46 (0)	1/121 (0.8)	0/26 (0)
TG12/TG12, 7T/7T	6/193 (3.1)	0/46 (0)	6/121 (5.0)	0/26 (0)
TG12/TG13, 5T/7T	4/193 (2.1)	2/46 (4.3)	1/121 (0.8)	1/26 (3.8)

CP chronic pancreatitis

rare variants in the *CFTR* gene. The c.1753G>T (p.E585X) variant is a nonsense variant, and the c.2869delC (p.L957fs) variant leads to a stop codon afterward at amino acid 967. These variants result in a heavily truncated protein missing nearly two-thirds (p.E585X) or more than one-third (p.L957fs) of its amino acids. Because we did not perform functional assays, we do not have direct evidence that these two variants cause loss of the CFTR expression and/or function. However, a general acknowledgment has been agreed that mutations of this type, called class I mutations, are associated with complete loss or near complete loss of the CFTR function (<3 % of wild-type CFTR function) [33, 34]. The pathogenic potential of another novel variant, c.1231A>G (p.K411E), is currently unknown, but the in silico analyses suggest that this variant is deleterious. Importantly, the clinical phenotype of this patient might be complicated by the presence of another variant, p.L1156F. Noone et al. [30] reported that pancreatitis risk was increased approximately 40-fold by having two *CFTR* mutations. This is also the case with the c.374T>C (p.I125T) variant. Two of the three patients carrying this variant had other non-synonymous variants (p.I556V and p.R1453W). This p.I125T variant was originally reported in Chinese patients with idiopathic bronchiectasis and considered to be associated with CFTR-RD [35].

There are considerable regional and ethnic variations in the spectrum of the *CFTR* mutations [15]. Approximately 70 % of individuals with CF in the Caucasian population are homozygous for the F508del mutation, and almost 90 % of the patients have at least one F508del allele [36]. This mutation is extremely rare in the Japanese population, accounting for the rare presentation of classical CF in this region (approximately 1/350,000 live births) [37]. It is not surprising that the CF-causing mutations are frequently found in Caucasians, but very rarely in East Asia. Audrézet et al. [29] reported from France that at least 20 % of the patients with idiopathic CP carried one of the most common *CFTR* mutations. Fujiki et al. [38] reported from Japan that none of the 20 common CF-causing mutations was found in 65 Japanese patients with CP (51 alcoholic and 14 idiopathic). Wang et al. [39] reported comprehensive screening of pancreatitis susceptibility genes including *CFTR* in 75 pediatric patients with idiopathic CP from China. They identified a novel 8-bp deletion in exon 4, but not the common CF-causing mutations. In this study, we found no common severe CF-causing mutations, in agreement with these previous studies from East Asia.

We found a significant association between the p.Q1352H variant and CP. This finding confirms the previous reports from Japan and Korea showing that this variant was over-presented in patients with CP compared to controls [38, 40]. Fujiki et al. [38] from Japan reported that the frequency of this variant was higher in patients with CP (8/65, 12.3 %) than in controls (6/162, 3.7 %). Lee et al. [40] reported from Korea that 14.3 % (4/28) of the patients with CP had this variant, whereas only 0.9 % (1/117) of the controls did. Glutamine at 1,352 is located in the second nucleotide-binding fold of CFTR, and its change to histidine (p.Q1352H) causes reductions in both the protein expression and channel activity of CFTR [40]. Similarly, we found that the p.L1156F variant was overexpressed in patients with CP. A functional study reported reduced Cl^-/HCO_3^- permeability in the presence of the p.L1156F variant [41].

Gene–gene interactions of known pancreatitis susceptibility genes, especially between the *CFTR* and *SPINK1* genes, have been increasingly recognized. Indeed, seven out of 25 patients carrying the *SPINK1* variant(s) had the *CFTR* p.Q1352H and/or p.L1156F variants. One patient was trans-heterozygous for the *CTRC* p.R29Q and *CFTR* p.I125T/p.L1156F variants. Noone et al. [30] reported that pancreatitis risk was increased approximately 40-fold by having two *CFTR* mutations, 20-fold by having the *SPINK1* p.N34S variant, and 900-fold by having both. Trans-heterozygosity of the *SPINK1* p.N34S with the

Table 8 Total *CFTR* sequencing results of patients with *SPINK1*, *PRSS1*, *CTRC*, or *CPA1* mutations

Case#	Etiology	*CFTR* variants[a]	c.1210-34TG(9_13) c.1210-12T(5_9)	*SPINK1*	*PRSS1*	*CTRC*	*CPA1*
B1	Familial	p.Q1352H/-	TG11/TG12, 7T/7T	p.N34S/p.N34S			
B2	Idiopathic	–	TG12/TG12, 7T/7T	p.N34S/p.N34S			
B3	Idiopathic	–	TG11/TG12, 7T/7T	p.N34S/p.N34S			
B4	Idiopathic	p.L1156F/-, p.Q1352H/-	TG11/TG11, 7T/7T	p.N34S/-			
B5	Idiopathic	p.Q1352H/-	TG11/TG12, 7T/7T	p.N34S/-			
B6	Idiopathic	p.Q1352H/-	TG11/TG12, 7T/7T	p.N34S/-			
B7	Idiopathic	–	TG11/TG12, 7T/7T	p.N34S/-			
B8	Idiopathic	–	TG11/TG12, 7T/7T	p.N34S/-			
B9	Idiopathic	–	TG11/TG12, 7T/7T	p.N34S/-			
B10	Idiopathic	–	TG11/TG12, 7T/7T	p.N34S/-			
B11	Idiopathic	–	TG11/TG12, 7T/7T	p.N34S/-			
B12	Idiopathic	–	TG11/TG12, 7T/7T	p.N34S/-			
B13	Idiopathic	–	TG11/TG12, 7T/7T	p.N34S/-			
B14	Alcoholic	–	TG12/TG13, 5T/7T	p.N34S/-			
B15	Idiopathic	–	TG11/TG12, 7T/7T	p.N34S/IVS3+2T>C			
B16	Idiopathic	p.R1453W/-	TG11/TG11, 7T/7T	p.N34S/IVS3+2T>C			
B17	Idiopathic	–	TG11/TG12, 7T/7T	IVS3+2T>C/IVS3+2T>C			
B18	Idiopathic	–	TG11/TG12, 7T/7T	IVS3+2T>C/IVS3+2T>C			
B19	Hereditary	p.I125T/-, p.L1156F/-	TG11/TG12, 5T/7T	IVS3+2T>C/-			
B20	Familial	p.L1156F/-	TG11/TG12, 7T/7T	IVS3+2T>C/-			
B21	Idiopathic	–	TG11/TG12, 7T/7T	IVS3+2T>C/-			
B22	Alcoholic	p.Q1352H/-	TG11/TG12, 7T/7T	IVS3+2T>C/-			
B23	Alcoholic	–	TG11/TG12, 7T/7T	IVS3+2T>C/-			
B24	Idiopathic	–	TG11/TG12, 7T/7T	p.P45S/-			
B25	Idiopathic	–	TG12/TG12, 7T/7T	IVS3+2T>C/-	p.R122H/-		
B26	Hereditary		TG11/TG12, 7T/7T		p.R122H/-		
B27	Idiopathic	p.I556V/-	TG11/TG12, 7T/7T		p.N29I/-		
B28	Idiopathic	p.I125T/-, p.L1156F/-	TG11/TG12, 7T/7T			p.R29Q/-	
B29	Idiopathic	–	TG11/TG12, 7T/7T				p.T368_Y369ins20/-

Nine patients had the non-synonymous *CFTR* variants, which are probably damaging based on the SIFT or the PolyPhen-2 prediction

The p.I556V variant appeared to be benign based on the SIFT or the PolyPhen-2 prediction

Case B28 is the same as A5 in Table 6

[a] We excluded the p.V470M variant from the list because of its similar frequencies in patients and controls

CFTR p.R75Q was reported to increase CP risk [31]. 6.5 % of the patients with idiopathic or hereditary CP carried variants in at least two pancreatitis susceptibility genes [32]. Whether the coinheritance of variants/mutations in pancreatitis susceptibility gene is a *bona fide* example of digenic inheritance or interaction between a disease-causing gene and a genetic modifier is unclear in most cases [42].

We used targeted sequence capture and high-throughput NGS to detect variants in the *CFTR* gene. Due to the large size (27 exons, 1,480 amino acids), traditional technologies, such as PCR and capillary sequencing, are time- and cost-consuming. A major advantage of the HaloPlex-targeted enrichment system is the convenient workflow, integrating both capture and library preparation. The protocol allows one person to prepare a set of finished libraries within two working days and requires no larger specialized instruments. Sequence capture eliminates the necessity of setting up hundreds of PCR, instead allowing for parallel

enrichment of target regions in a single experiment. A weakness of this method is that the detection of larger copy number variations would require different methods. We have designed the HaloPlex platform for more than 70 genes, including the known pancreatitis susceptibility genes such as *CFTR*, *PRSS1*, *SPINK1*, *CTRC,* and *CPA1*. This system has allowed us to perform rapid screening of the known susceptibility genes simultaneously and gives an overview of potentially pathogenic variants in patients with pancreatitis. In addition, our HaloPlex platform includes candidates of novel pancreatitis susceptibility genes such as pancreatic digestive enzymes, those highly expressed in the pancreas and those related to autophagy and endoplasmic reticulum stress. This system might contribute to the identification of novel pancreatitis susceptibility genes in the future.

Acknowledgments The authors are grateful to Ms. Yoko Tateda for the excellent technical assistance. This work was supported in part by the Pancreas Research Foundation of Japan (to E. Nakano), the HIROMI Medical Research Foundation (to A. Masamune), the Mother and Child Health Foundation (to A. Masamune), the Smoking Research Foundation (to A. Masamune), and by the Ministry of Health, Labour, and Welfare of Japan.

Conflict of interest None.

References

1. Steer ML, Waxman I, Freedman S. Chronic pancreatitis. *N Engl J Med.* 1995;332:1482–1490.
2. Witt H, Apte MV, Keim V, Wilson JS. Chronic pancreatitis: challenges and advances in pathogenesis, genetics, diagnosis, and therapy. *Gastroenterology.* 2007;132:1557–1573.
3. Whitcomb DC, Gorry MC, Preston RA, et al. Hereditary pancreatitis is caused by a mutation in the cationic trypsinogen gene. *Nat Genet.* 1996;14:141–145.
4. Witt H, Luck W, Hennies HC, et al. Mutations in the gene encoding the serine protease inhibitor, Kazal type 1 are associated with chronic pancreatitis. *Nat Genet.* 2000;25:213–216.
5. Rosendahl J, Witt H, Szmola R, et al. Chymotrypsin C (CTRC) variants that diminish activity or secretion are associated with chronic pancreatitis. *Nat Genet.* 2008;40:78–82.
6. Witt H, Beer S, Rosendahl J, et al. Variants in CPA1 are strongly associated with early onset chronic pancreatitis. *Nat Genet.* 2013;45:1216–1220.
7. Masamune A. Genetics of pancreatitis: the 2014 update. *Tohoku J Exp Med.* 2014;232:69–77.
8. Kume K, Masamune A, Mizutamari H, et al. Mutations in the serine protease inhibitor Kazal Type 1 (SPINK1) gene in Japanese patients with pancreatitis. *Pancreatology.* 2005;5:354–360.
9. Masamune A, Nakano E, Kume K, Kakuta Y, Ariga H, Shimosegawa T. Identification of novel missense CTRC variants in Japanese patients with chronic pancreatitis. *Gut.* 2013;62:653–654.
10. Masamune A, Nakano E, Kume K, Takikawa T, Kakuta Y, Shimosegawa T. PRSS1 c.623G>C (p.G208A) variant is associated with pancreatitis in Japan. *Gut.* 2014;63:336.
11. Sharer N, Schwarz M, Malone G, et al. Mutations of the cystic fibrosis gene in patients with chronic pancreatitis. *N Engl J Med.* 1998;339:645–652.
12. Cohn JA, Friedman KJ, Noone PG, Knowles MR, Silverman LM, Jowell PS. Relation between mutations of the cystic fibrosis gene and idiopathic pancreatitis. *N Engl J Med.* 1998;339:653–658.
13. Bombieri C, Claustres M, De Boeck K, et al. Recommendations for the classification of diseases as CFTR-related disorders. *J Cyst Fibros.* 2011;10:S86–S102.
14. Riordan JR, Rommens JM, Kerem B, et al. Identification of the cystic fibrosis gene: cloning and characterization of complementary DNA. *Science.* 1989;245:1066–1073.
15. Ratjen F, Döring G. Cystic fibrosis. *Lancet.* 2003;361:681–689.
16. Dequeker E, Stuhrmann M, Morris MA, et al. Best practice guidelines for molecular genetic diagnosis of cystic fibrosis and CFTR-related disorders–updated European recommendations. *Eur J Hum Genet.* 2009;17:51–65.
17. Metzker ML. Sequencing technologies-the next generation. *Nat Rev Genet.* 2009;11:31–46.
18. Gilissen C, Hoischen A, Brunner HG, Veltman JA. Unlocking Mendelian disease using exome sequencing. *Genome Biol.* 2011;12:228.
19. Do R, Kathiresan S, Abecasis GR. Exome sequencing and complex disease: practical aspects of rare variant association studies. *Hum Mol Genet.* 2012;21:R1–R9.
20. Myllykangas S, Ji HP. Targeted deep resequencing of the human cancer genome using next-generation technologies. *Biotechnol Genet Eng Rev.* 2010;27:135–158.
21. Berglund EC, Lindqvist CM, Hayat S, et al. Accurate detection of subclonal single nucleotide variants in whole genome amplified and pooled cancer samples using HaloPlex target enrichment. *BMC Genom.* 2013;14:856.
22. Mertes F, Elsharawy A, Sauer S, et al. Targeted enrichment of genomic DNA regions for next-generation sequencing. *Brief Funct Genomics.* 2011;10:374–386.
23. Etemad B, Whitcomb DC. Chronic pancreatitis: diagnosis, classification, and new genetic developments. *Gastroenterology.* 2001;120:682–707.
24. Howes N, Lerch MM, Greenhalf W, et al. European Registry of Hereditary Pancreatitis and Pancreatic Cancer (EUROPAC). Clinical and genetic characteristics of hereditary pancreatitis in Europe. *Clin Gastroenterol Hepatol.* 2004;2:252–261.
25. Nishimori I, Kamakura M, Fujikawa-Adachi K, et al. Mutations in exons 2 and 3 of the cationic trypsinogen gene in Japanese families with hereditary pancreatitis. *Gut.* 1999;44:259–263.
26. Sunyaev S, Ramensky V, Koch I, Lathe W III, Kondrashov AS, Bork P. Prediction of deleterious human alleles. *Hum Mol Genet.* 2001;10:591–597.
27. Dorfman R, Nalpathamkalam T, Taylor C, et al. Do common in silico tools predict the clinical consequences of amino-acid substitutions in the CFTR gene? *Clin Genet.* 2010;77:464–473.
28. Steiner B, Rosendahl J, Witt H, et al. Common CFTR haplotypes and susceptibility to chronic pancreatitis and congenital bilateral absence of the vas deferens. *Hum Mutat.* 2011;32:912–920.
29. Audrézet MP, Chen JM, Le Maréchal C, et al. Determination of the relative contribution of three genes-the cystic fibrosis transmembrane conductance regulator gene, the cationic trypsinogen gene, and the pancreatic secretory trypsin inhibitor gene-to the etiology of idiopathic chronic pancreatitis. *Eur J Hum Genet.* 2002;10:100–106.
30. Noone PG, Zhou Z, Silverman LM, Jowell PS, Knowles MR, Cohn JA. Cystic fibrosis gene mutations and pancreatitis risk: relation to epithelial ion transport and trypsin inhibitor gene mutations. *Gastroenterology.* 2001;121:1310–1319.
31. Schneider A, Larusch J, Sun X, et al. Combined bicarbonate conductance-impairing variants in CFTR and SPINK1 variants are associated with chronic pancreatitis in patients without cystic fibrosis. *Gastroenterology.* 2011;140:162–171.

32. Rosendahl J, Landt O, Bernadova J, et al. CFTR, SPINK1, CTRC and PRSS1 variants in chronic pancreatitis: is the role of mutated CFTR overestimated? *Gut*. 2013;62:582–592.
33. Welsh MJ, Smith AE. Molecular mechanisms of CFTR chloride channel dysfunction in cystic fibrosis. *Cell*. 1993;73:1251–1254.
34. Castellani C, Cuppens H, Macek M Jr, et al. Consensus on the use and interpretation of cystic fibrosis mutation analysis in clinical practice. *J Cyst Fibros*. 2008;7:179–196.
35. Ngiam NS, Chong SS, Shek LP, et al. Cystic fibrosis transmembrane conductance regulator (CFTR) gene mutations in Asians with chronic pulmonary disease: a pilot study. *J Cyst Fibros*. 2006;5:159–164.
36. Watson MS, Cutting GR, Desnick RJ, et al. Cystic fibrosis population carrier screening: 2004 revision of American College of Medical Genetics mutation panel. *Genet Med*. 2004;6:387–391.
37. Yamashiro Y, Shimizu T, Oguchi S, Shioya T, Nagata S, Ohtsuka Y. The estimated incidence of cystic fibrosis in Japan. *J Pediatr Gastroenterol Nutr*. 1997;24:544–547.
38. Fujiki K, Ishiguro H, Ko SB, et al. Genetic evidence for CFTR dysfunction in Japanese: background for chronic pancreatitis. *J Med Genet*. 2004;41:e55.
39. Wang W, Sun XT, Weng XL, et al. Comprehensive screening for PRSS1, SPINK1, CFTR, CTRC and CLDN2 gene mutations in Chinese paediatric patients with idiopathic chronic pancreatitis: a cohort study. *BMJ Open*. 2013;3:e003150.
40. Lee JH, Choi JH, Namkung W, et al. A haplotype-based molecular analysis of CFTR mutations associated with respiratory and pancreatic diseases. *Hum Mol Genet*. 2003;12:2321–2332.
41. Ko S, Zeng W, Fujiki K, et al. Functional characterization of L1156F CFTR: a newly identified mutation in Japanese patients with chronic pancreatitis. *J Physiol Sci*. 2006;56:S71. (abstract).
42. Chen JM, Férec C. Chronic pancreatitis: genetics and pathogenesis. *Annu Rev Genomics Hum Genet*. 2009;10:63–87.

ELSEVIER

Cancer Genetics ■ (2014) ■

Cancer Genetics

Analysis of the t(3;8) of hereditary renal cell carcinoma: a palindrome-mediated translocation

Takema Kato [a], Colleen P. Franconi [a], Molly B. Sheridan [a], April M. Hacker [a], Hidehito Inagakai [b], Thomas W. Glover [c], Martin F. Arlt [c], Harry A. Drabkin [d], Robert M. Gemmill [d], Hiroki Kurahashi [b], Beverly S. Emanuel [a,e,*]

[a] *Division of Human Genetics, The Children's Hospital of Philadelphia, Philadelphia, PA, USA;* [b] *Division of Molecular Genetics, Institute for Comprehensive Medical Science, Fujita Health University, Aichi, Japan;* [c] *Department of Human Genetics, University of Michigan, Ann Arbor, MI, USA;* [d] *Division of Hematology-Oncology, Medical University of South Carolina, Charleston, SC, USA;* [e] *Department of Pediatrics, The Perelman School of Medicine at the University of Pennsylvania, Philadelphia, PA, USA*

It has emerged that palindrome-mediated genomic instability generates DNA-based rearrangements. The presence of palindromic AT-rich repeats (PATRRs) at the translocation breakpoints suggested a palindrome-mediated mechanism in the generation of several recurrent constitutional rearrangements: the t(11;22), t(17;22), and t(8;22). To date, all reported PATRR-mediated translocations include the PATRR on chromosome 22 (PATRR22) as a translocation partner. Here, the constitutional rearrangement, t(3;8)(p14.2;q24.1), segregating with renal cell carcinoma in two families, is examined. The chromosome 8 breakpoint lies in PATRR8 in the first intron of the *RNF139* (*TRC8*) gene, whereas the chromosome 3 breakpoint is located in an AT-rich palindromic sequence in intron 3 of the *FHIT* gene (PATRR3). Thus, the t(3;8) is the first PATRR-mediated, recurrent, constitutional translocation that does not involve PATRR22. Furthermore, we detect de novo translocations similar to the t(11;22) and t(8;22), involving PATRR3 in normal sperm. The breakpoint on chromosome 3 is in proximity to FRA3B, the most common fragile site in the human genome and a site of frequent deletions in tumor cells. However, the lack of involvement of PATRR3 sequence in numerous FRA3B-related deletions suggests that there are several different DNA sequence–based etiologies responsible for chromosome 3p14.2 genomic rearrangements.

Keywords Palindrome, PATRR, translocation, FRA3B, renal cell carcinoma

Multiple types of repetitive sequence are abundant in the human genome. They are capable of forming various non-B DNA structures, which frequently induce genomic instability and rearrangements (1–4). Palindromic sequences or inverted repeats represent an unstable DNA motif because they can induce unusual stem-loop DNA structures (5,6). Such repetitive sequences are often responsible for inducing spontaneously arising genomic rearrangements such as recombination or deletion in model organisms (7–9).

Palindromic AT-rich repeat (PATRR)–mediated translocations are an extensively described form of repetitive DNA instability. Previously, recurrent translocations at 22q11 including the constitutional t(11;22)(q23;q11), t(8;22)(q24;q11), and t(17;22)(q11;q11) have been reported. The presence of PATRRs at 22q11, as well as within the relevant 11q23, 8q24, and 17q11 regions, suggests a PATRR-mediated etiology for these recurrent constitutional translocations with 22q11. These translocations have been reported in unrelated families, and the breakpoints in almost all translocation carriers are localized at the center of the PATRR on both chromosomes (10–15). Similarly, a t(1;22)(q21;q11), t(9;22)(p21;q11) and a t(4;22)(q35;q11), all nonrecurrent translocations, were reported as PATRR mediated (16–18). To date, all PATRR-mediated translocations have involved the PATRR on chromosome 22 (PATRR22). Therefore, PATRR22 represents a hot spot for constitutional translocations (19). However, in this manuscript, the first PATRR-mediated translocation that does not involve PATRR22 is described. The constitutional t(3;8)(p14.2;q24.2) has previously been associated with the inheritance of renal cell carcinoma in two unrelated families (20,21). The t(3;8) balanced

Received December 30, 2013; received in revised form February 7, 2014; accepted March 10, 2014.
* Corresponding author.
E-mail address: beverly@mail.med.upenn.edu

2210-7762/$ - see front matter © 2014 Elsevier Inc. All rights reserved.
http://dx.doi.org/10.1016/j.cancergen.2014.03.004

carriers have breakpoints in the 5′ untranslated region (UTR) of *FHIT* on chromosome 3 and in the sterol-sensing domain of *RNF139* (*TRC8*) on chromosome 8 (21,22). Although it was known that the short arm of chromosome 3 is altered by deletions or translocations in renal cell carcinoma, until this study, the t(3;8) breakpoints were uncharacterized at the nucleotide level.

Previously, it was known that the t(3;8) breakpoint on chromosome 3 either coincides with or is close to FRA3B, the most common fragile site in the human genome, but the precise distance between the 3p translocation breakpoint and the fragile site was not known (23–26). Common fragile sites are specific chromosomal regions that preferentially exhibit chromosome instability that is visible on mitotic chromosomes as nonrandom gaps, constrictions, or breaks following partial inhibition of DNA synthesis. The gaps coincide with regions of deletions and intra- and interchromosomal recombination (27,28). Numerous heterozygous and homozygous deletions in various human cancers and precancerous lesions involve FRA3B, spanning *FHIT* introns 3–7 (29). Thus, it has been suggested that the presence of FRA3B may predispose chromosomes to the t(3;8) as well as to FRA3B deletions (30).

Here we characterize the t(3;8) breakpoint junctions and confirm that this is a palindrome-mediated translocation with a breakpoint localized to a newly described PATRR on chromosome 3 (PATRR3). PATRR3 and its surrounding sequence in translocation carriers and normal human samples have been examined and characterized. We also report detection of de novo translocations mediated by PATRR3 in sperm samples from normal males. Although the PATRR3 sequence is capable of adopting a secondary structure, FRA3B deletions do not encompass PATRR3. These analyses contribute to an understanding of the mechanisms responsible for PATRR-induced genomic rearrangements. These studies indicate that PATRR3-mediated translocations appear to be unrelated to FRA3B deletions, which lie in close proximity to, but distal to, PATRR3.

Materials and methods

Sequence analysis of the t(3;8) junction fragments and the breakpoint region

Control samples were collected through the clinical cytogenetics laboratory at the Children's Hospital of Philadelphia with proper institutional review board (IRB) approval and patient consent or they were purchased from the Coriell Institute for Medical Research. Genomic DNA was extracted from blood, lymphoblast, or fibroblast cell lines using the PureGene DNA purification kit (QIAGEN, Valencia, CA). The patients varied in ethnicity to include 12 Caucasians, two African Americans, two biracial individuals, and one Asian. The human–mouse chromosome 3–only somatic cell hybrid cell line (GM11713) was obtained from the Coriell Mutant Cell Repository. To narrow the location of the breakpoints, PCRs were performed to analyze sequences located on the derivative human chromosome 3 in a somatic cell hybrid. The der(3)t(3;8)- and der(8)t(3;8)-specific PCRs were performed as described in previous articles (31,32), differing only in primer selection. PCR products were purified by ExoSap-IT (GE Healthcare, Pittsburgh,PA) and sequenced bidirectionally by an ABI Prism Sequencer 3730 (Life Technologies, Grand Island, NY). The resulting sequences were aligned with PATRR3 and PATRR8 sequences. The PCR primers are listed in Table 1.

Table 1 Primer sequences

Chromosome Region	Primer	Sequence 5′ to 3′
Surround PATRR3	FHITi3-4F	GTTCCCCTTGAAATCACTGC
	FHITi3-4R	AGGTTACCAAAGTGATCAAACC
Surround PATRR3	FHITi3-5F	CACAAGGCTCACCACTAATCG
	FHITi3-5R	GCCGCTAAAACAATTCTTCC
Surround PATRR8	RNF139i1-1F	TTATTTGTCTATCTGATGCCTTCC
	RNF139i1-1R	CATGGAAGGTAACAAGAAAATGG
Surround PATRR8	RNF139i1-2F	TTAGTGGCCCATTTTCTTGG
	RNF139i1-2R	CAGTAGACGCATTTCACAATCC
PATRR3	PATRR3-386F	GCACCCTGAAGGCTACTTGTTAAAG
	PATRR3+411R	AACTGGGCTGGACCTCTTTTGGAAC
PATRR3 nested PCR	PATRR3 NestFw	AACTGGGCTGGACCTCTTTTGGAAC
	PATRR3 NestRv	GGCGCAAAAAAAARAAAGATATATGATATG
der(3)t(3;8)	PATRR3+411R	AACTGGGCTGGACCTCTTTTGGAAC
	PATRR8+267R	CATTTAAGTGATGACTCTGTCCAGGG
der(8)t(3;8)	PATRR8-512F	GATTACATATGGCATCTGGTAGGCTG
	PATRR3-386F	GCACCCTGAAGGCTACTTGTTAAAG
der(3)t(3;22)	PATRR3+411R	AACTGGGCTGGACCTCTTTTGGAAC
	JF22	CCTCCAACGGATCCATACT
der(22)t(3;22)	JF22	CCTCCAACGGATCCATACT
	PATRR3-386F	GCACCCTGAAGGCTACTTGTTAAAG
der(3)t(3;11)	PATRR3+411R	AACTGGGCTGGACCTCTTTTGGAAC
	PATRR11-216F	GAGAGTAAAGAAATAGTTCAGAAAGG
der(11)t(3;11)	PATRR11+212R	CCACAGACTCATTCATGGAACC
	PATRR3-386F	GCACCCTGAAGGCTACTTGTTAAAG

PATRR3 genotyping

For analysis of PATRR3 polymorphisms, genomic DNA was extracted from buccal cells or blood samples as described in the previous section. The PATRR3 region was amplified by PCR with the use of KOD Xtreme Hot Start DNA Polymerase (EMD4Biosciences, Billerica, MA). PCR cycles were as follows: 94°C for 2.5 minutes, 35 cycles at 98°C for 10 seconds and 63°C for 5 minutes, followed by a final extension at 63°C for 10 minutes. PCR products were separated by agarose gel electrophoresis, and then gel slices were purified by a QIAquick Gel Extraction Kit (QIAGEN). Nested PCR was performed on the gel-purified DNA to determine the size of the PATRR3. The PCR and nested PCR primers are listed in Table 1. The products of nested PCR reactions were sequenced directly using an ABI Prism Sequencer 3730 (Life Technologies).

Detection of a PATRR3 involved de novo translocation in normal males

Semen samples were acquired, with IRB approval, from individual anonymous donors with various genotypes of PATRR3. Testis samples were acquired, with IRB approval, from the Cooperative Human Tissue Network. Genomic DNA was extracted from semen or testis samples, and translocation-specific PCRs were performed as described in the previous sections. Primers for detection of PATRR-mediated translocations have been previously described and are listed in Table 1 (15,32). Multiple batches of 100-ng sperm DNA each containing 33,000 haploids were amplified. The frequency of translocation events was calculated in the following manner. The number of positive PCR reactions per total number of reactions was counted. The frequency was calculated on the basis that the probability of a positive PCR reaction corresponds to a total sum of a binomial series of the translocation frequency calculated using the equation $q=1-(1-p)^{1/n}$ as described previously (31).

Single nucleotide polymorphism arrays for detection of FRA3B deletions

Genomic DNA was extracted from cultured fibroblasts or peripheral blood. DNA quality was assessed by a NanoDrop Spectrometer (Thermo Fisher Scientific, Waltham, MA) and gel electrophoresis. Single nucleotide polymorphism (SNP) array analysis was performed using the Illumina Quad610 genotyping bead chip (Illumina, San Diego, CA) (33). Structural aberrations and copy number differences were visually detected using Illumina's BeadStudio software. The average resolution across the genome for the Illumina platform is 4 kb per SNP. To be confident of a duplication or deletion, 10 kb was a minimum requirement. The B allele frequency and log R ratio were used to determine copy number changes.

Results

Characterization of the t(3;8) breakpoints

Previously, the breakpoint locations of the t(3;8) were narrowed to the third intron of the *FHIT* gene located on chromosome 3 and the first intron of the *RNF139* gene on chromosome 8 (21,22) (Supplementary Figure 1). Since a PATRR on chromosome 8 (PATRR8), the breakpoint of the recurrent t(8;22), is also located in the first intron of *RNF139*, we hypothesized that the breakpoint of the t(3;8) might also reside in PATRR8. To further characterize the breakpoint, we utilized DNA from a somatic cell hybrid containing the human der(3)t(3;8). We used multiple sets of PCR primers in the vicinity of PATRR8 (Figure 1A) and in *FHIT* intron 3 (Figure 1B) to narrow the chromosome breakpoint regions to a 0.6-kb region on the derivative chromosome 8 and a 2.6-kb region of chromosome 8 on the der(3) that included PATRR8. Interestingly, the chromosome 3 breakpoint region contained an AT-rich region, suggesting that this region may also contain a PATRR.

Cell lines derived from the originally reported t(3;8) subjects were used to determine the translocation breakpoints (21,22). Despite being unrelated, translocations segregating in these two families have grossly the same breakpoints. Translocation-specific PCR and DNA sequencing were performed as previously described (31) (Figure 1C). DNA sequences from carriers in both families demonstrated almost identical breakpoints in the PATRR8 region. The chromosome 3 breakpoint was reconstructed using junction fragment sequences because an intact sequence was not present in the reference genomes available. Since access to the individuals in whom the t(3;8) originally arose is unavailable for further analysis, we cannot rule out the possibility that the reconstructed PATRR sequence is incorrect and has been altered by DNA resection during translocation. Nonetheless, this reconstructed breakpoint includes a novel PATRR sequence, which consists of variable number tandem repeats (VNTRs) and $(AT)_n$ sequences. The reconstructed PATRR3 from the carriers differ from one another and are about 750 bp (AB690558) and 600 bp (AB690559) in length. They are predicted to have symmetrical hairpin structures by the M-fold software program (http://mfold.rna.albany.edu/?q=mfold) (34) (Supplementary Figure 2A). We suggest that these palindromic sequences contribute to the genomic instability of PATRR3, leading to unusual DNA structures.

The t(3;8) breakpoint on chromosome 3 is either localized in or close to the FRA3B region, which has been associated with deletions in various tumor cells (22,30,35). To confirm that the t(3;8) did not induce copy number changes in the FRA3B region, we performed a SNP array using DNA from each of the translocation carriers. This analysis did not identify copy number alterations at either 3p14 in the FRA3B region or at the chromosome 8 breakpoint region (Supplementary Figure 3). Thus, as is the case with other PATRR-mediated translocations, the t(3;8)s appear to be balanced translocations that do not result in a gain or loss of genetic material (14,15,36).

Polymorphisms of PATRR3 sequences and their structures

To further characterize PATRR3 sequence variation, we performed extensive genotyping using DNA from several human ethnic groups. As reported previously, PATRRs are often polymorphic in size (15,32,37,38). PCR results reveal that PATRR3 is hypervariable in length among individuals, and ranges from 600 to 2030 bp (Figure 2). Sequence analysis demonstrates that all of the samples have different fragment lengths, despite the fact that different alleles appear to be the

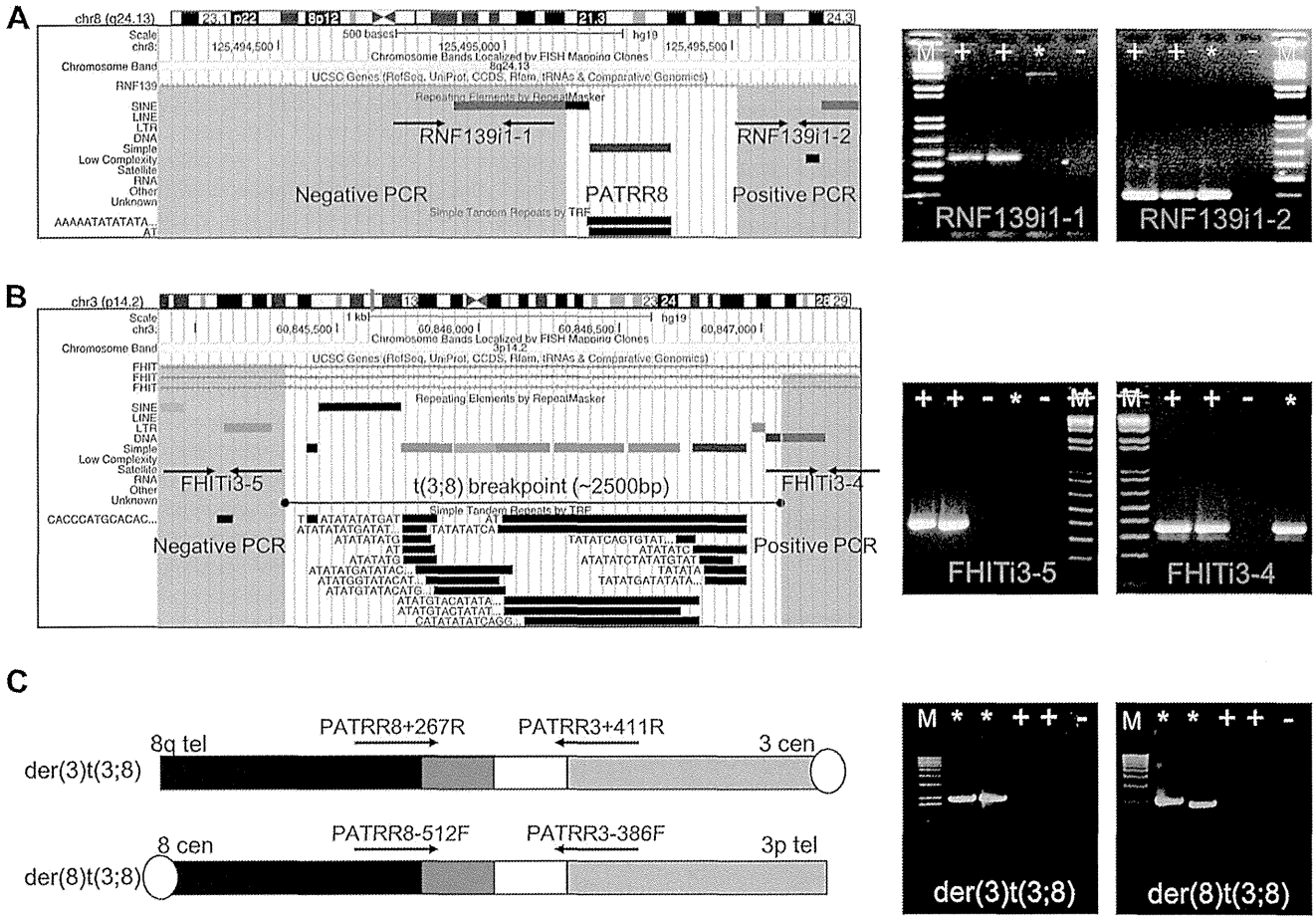

Figure 1 Determination of the breakpoints of the t(3;8). (A) t(3;8) breakpoint mapping on chromosome 8 with DNA from der(3)t(3;8) somatic cell hybrid. On the left is the ideogram of chromosome 8 with a screenshot from the University of California Santa Cruz (UCSC) genome browser below in the region containing the PATRR in the *RNF139* gene. On the right are the relevant PCR results. (B) t(3;8) breakpoint mapping on chromosome 3 with DNA from der(3)t(3;8) somatic cell hybrid. On the left is the ideogram of chromosome 3, with a screenshot from the UCSC genome browser below it, in the region containing PATRR3 in the *FHIT* gene. On the right are the relevant PCR results. Lane +, healthy control; lane *, der(3)t(3;8) hybrid cell; lane −, negative control; lane M, 1 kb+ladder. Sequences surrounding the breakpoints were visualized in the UCSC genome browser. (C) PCR results for detection of the breakpoint region of the t(3;8) translocation in a balanced carrier. Primer locations are shown as arrows above the chromosomes. The black bar indicates chromosome 8q, the red bar the chromosome 8 PATRR, the white bar indicates the chromosome 3 PATRR, and the gray bar chromosome 3p. Lane +, healthy control; lane *, t(3;8) carrier; lane −, negative control; lane M, 1 kb+ladder. *Abbreviations*: RNF139i1-1, primer name; RNF139i1-2, primer name; TRF, Tandem Repeat Finder; tel, telomere; cen, centromere.

same length by gel electrophoresis. We found only one symmetrical PATRR3 (S-PATRR3), whereas all other alleles contain an asymmetrical PATRR3 (AS-PATRR3). The potential secondary structure of each of the PATRR3 sequences was predicted using the M-fold software program (34) (Supplementary Figure 2B). The S-PATRR3 is composed of a symmetrical long hairpin structure, whereas AS-PATRR3s appear to have shorter hairpin structures of various lengths. The number and/or orientation of the VNTRs and $(AT)_n$ length contribute to differences in size and secondary structure-forming propensity.

Translocation-specific PCR using normal human sperm

We have previously demonstrated that de novo t(11;22)s occur frequently in sperm from normal healthy males (31). Recently, we also identified de novo PATRR-mediated t(8;22)s as well as t(8;11)s by a similar PCR method, suggesting that a proportion of constitutional translocations result from a palindrome-mediated mechanism in meiosis (15). Here we tried to detect de novo occurrences of PATRR3-involved translocations by PCR in sperm from normal healthy males with various PATRR3 alleles (Figure 3A). First, we performed der(3)t(3;8) and der(8)t(3;8) translocation–specific PCR in sperm samples. However, neither the der(3)t(3;8) nor der(8)t(3;8) was observed in any of our samples (translocation frequency $< 3.4 \times 10^{-7}$). Despite the fact that the t(3;22) and t(3;11) have not been reported in the literature, the t(3;22) and t(3;11) were detected (Figure 3B) at a low translocation frequency ($\leq 10^{-6}$) in a sperm sample derived from a heterozygous S-PATRR3 carrier. Sequence analysis revealed that all of the translocations appear to originate from the S-PATRR3 allele (5595b). Sperm samples from carriers of AS-PATRR3s (5804) on both chromosomes did not produce any de novo PATRR3 related translocations, or produced such a small

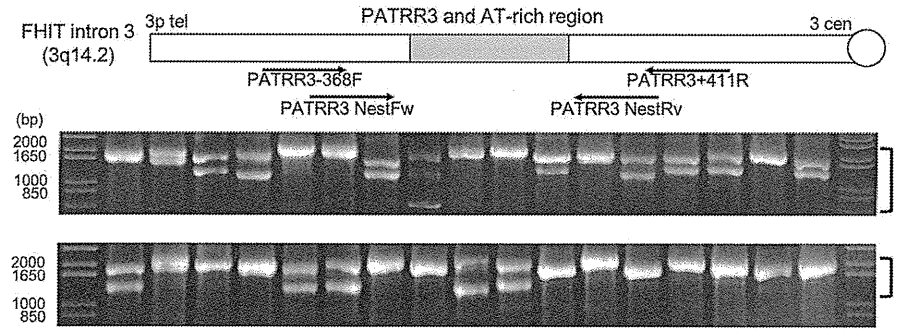

Figure 2 Genotyping human PATRR3 by PCR to determine PATRR3 polymorphisms. Agarose gel electrophoresis of nested PCR products from 17 normal human samples. Primer locations for PCR and nested PCR are depicted below the chromosome. The bracketed text beside the gel indicates the PATRR3 product(s). *Abbreviations*: NestFw: nested forward primer; NestRw: nested reverse primer.

number of de novo translocations that they were below the sensitivity of this PCR assay. However, de novo t(11;22) and t(8;22) from these individuals could be detected by PCR. Thus, given the caveat that we found only one individual with an S-PATTR3 allele, the occurrence of de novo PATRR3-involved translocations appears to be dependent on the presence of PATRR3 symmetry.

Genomic analysis of the FRA3B region

Sequence analysis using the M-fold program indicates that PATRR3s are predicted to adopt secondary structures, with the potential for impeding replication fork progression (Supplementary Figure 2). FRA3B-related deletions, which are induced by aphidicolin (APH), appear to be located in the t(3;8) breakpoint region (39). Furthermore, APH-induced deletions have been detected in the PATRR on chromosome 11 (PATRR11) (40). These observations suggested that PATRR3 sequences might form unusual structures and induce recurrent FRA3B deletions. To determine whether a PATRR3 sequence is involved in FRA3B deletions, we analyzed human samples with deletions in the vicinity of FRA3B and DNA from a chromosome 3–only human–mouse somatic cell hybrid with an intact FRA3B region. The somatic cell hybrid contains one normal human chromosome 3 and was not initially treated with APH. First, using array data derived from 2,067 healthy controls (41), we assessed copy number variation in the FRA3B region. Many deletions in the FRA3B region were observed, yet none appeared to include PATRR3. Recurrent deletions were concentrated in intron 5 of the *FHIT* gene (Figure 4A). In a previous study, Durkin et al., using the same chromosome 3 human–mouse somatic cell hybrid, established that deletions in the FRA3B region are induced upon APH-mediated replication stress (29). Using the hybrid clones containing APH-induced deletions, PCR was performed to determine whether the PATRR3 region is retained. All clones retain PATRR3 (Figure 4B). Of note, the PATRR3 sequence of the human–mouse somatic cell hybrid is AS-PATRR3 (AB690564). Despite the AS-PATRR3 allele type, many FRA3B deletions were seen. These results indicate that

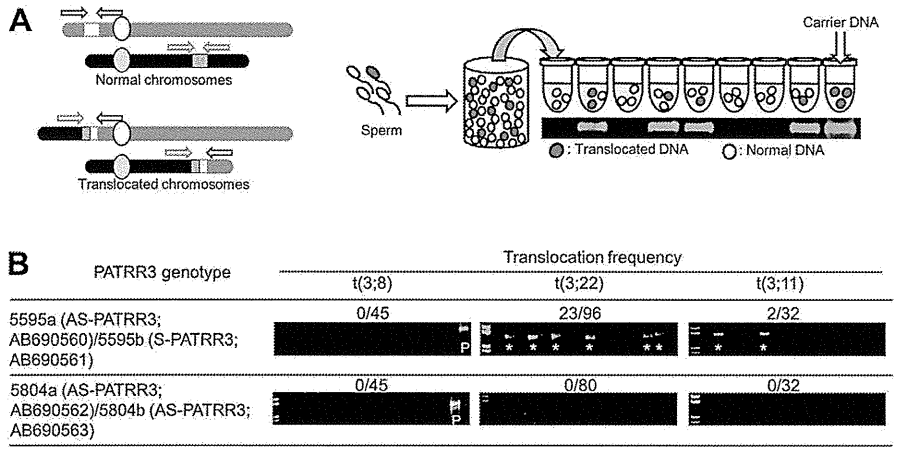

Figure 3 Detection of de novo PATRR3-involved translocations. (A) The illustration on the left shows the strategy of translocation-specific PCR. Arrowheads indicate each relevant primer. The illustration on the right is a diagram of the strategy used for estimation of translocation frequency by PCR. Genomic DNA was isolated from sperm samples. Translocation-specific PCR was performed using multiple batches of template DNA. Additional details of the methodology are described in the Materials and methods section. The gel images show representative PCR results derived from sperm DNA samples. (B) Translocation frequency of PATRR3-related PCR. Lane *, PCR positive; Lane P, t(3;8) carrier. PCR products from 200ng of sperm DNA.

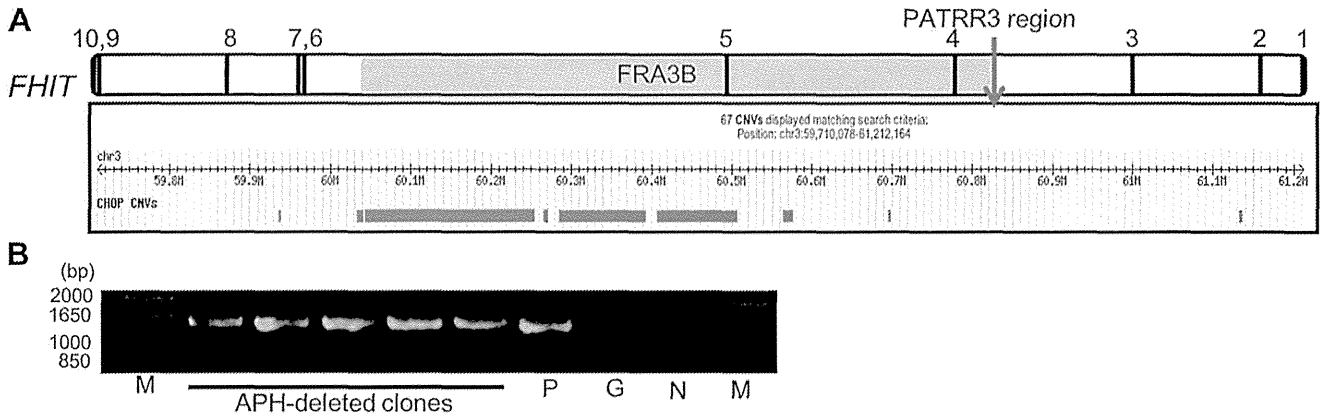

Figure 4 Copy number variations (CNVs) in the *FHIT* gene. (A) FRA3B deletions in 2,067 samples from healthy individuals are illustrated. Deletions are depicted under the genomic position. Green bars indicate recurrent deletions. Red bars indicate unique deletions. In total, 61 deletions were found in the *FHIT* gene. Among them, 55 deletions were not unique (green bars 2+6+47). Indicated by the red bars are the unique deletions. (B) PCR results for the PATRR3 region in APH-induced FRA3B deletions. Lane P, chromosome 3 hybrid DNA (non–APH-treated); lane M, 1 kb+ladder; lane G, mouse genomic DNA; lane N, negative control. *Abbreviation*: CHOP, Children's Hospital of Philadelphia.

deletions of FRA3B do not include PATRR3, suggesting that a PATRR3 sequence might not induce the FRA3B deletions.

Discussion

In this study, a recurrent, constitutional PATRR-mediated translocation, which does not involve PATRR22, has been examined in two unrelated families. This translocation, the t(3;8)(p14.2;q24.1), has previously been associated with hereditary renal cell carcinoma in these individuals and their translocation carrier relatives. Intriguingly, the breakpoint sequence of chromosome 8 in the t(3;8) is in the same region as the recurrent t(8;22) breakpoint (15). Also, the breakpoint of chromosome 3 is localized at the center of a novel AT-rich palindromic sequence (Figures 1A and 1B). Neither translocation carrier demonstrates DNA deletions surrounding the breakpoint regions (Supplementary Figure 3). Collectively, these findings indicate that the t(3;8) is another constitutional, recurrent, and balanced PATRR-mediated translocation. Reconstructing the original chromosome 3 region from the der(3) and der(8) junction fragments reveals that PATRR3 consists of a combination of many VNTRs and $(AT)_n$ sequences that form an inverted repeat. In the general population, PATRR3 varies in size and sequence. The majority of human PATRR3 alleles are asymmetric and appear to have arisen either by deletion of a symmetrical allele or by transmission with minor nucleotide substitutions (42).

The frequency of de novo PATRR3-related translocations is relatively low, compared with that of the t(11;22) and t(8;22) (15,32). Despite the possibility of PATRR3 having the longest palindromic sequence, de novo translocations are rarely seen (43). We have observed that PATRR3 has several large mismatches between its proximal and distal arms and a relatively low AT content (about 75%) compared with that of other PATRRs. The AT content of a PATRR greatly affects its predicted propensity to form secondary structures. A low melting temperature would be expected to permit double-stranded DNA to denature more readily, allowing the subsequent formation of a single-stranded folded structure (44,45). Thus, as a result of its lower AT content, PATRR3 might be less likely to form a cruciform structure than other PATRRs. Consequently, de novo PATRR3-related translocations may be produced infrequently in sperm (46).

De novo translocations between PATRR3 and other PATRRs [t(3;22) and t(3;11)] were seen as PCR products only in the sperm sample carrying the symmetrical PATRR3 allele, even though neither of these translocations has been reported in the literature. In contrast, de novo t(3;8)s have not been detected in sperm, despite the fact that several balanced translocation carriers have been reported. Prior to the present t(3;8) findings, all of the PATRR-mediated translocations had included PATRR22 as a partner (43,47). This finding suggests that there may be a hierarchy of susceptibility to translocation that is likely based on the configuration of both of the partner PATRRs.

In fact, numerous t(11;22) carriers have been reported (10,36,48,49). Therefore, it appears that the most translocation-vulnerable PATRR is PATRR22, with the next most susceptible being the PATRR11. PATRR11- and 22-related translocations are observed at a high frequency in sperm samples (32,38). Similarly, t(8;22) carriers have been reported in at least 12 unique cases, and the t(8;22) arises in sperm at a frequency of approximately 2×10^{-6}. The hypothetical t(8;11) rearrangement is also identified in sperm, albeit infrequently (15). Previous studies indicate that PATRR8 is less susceptible to translocation than are PATRR11 and 22, which seems to mirror the experience related to occurrence of PATRR3-related translocations. It supports the observation that de novo t(3;8)s did not take place or were produced so infrequently that they were below the sensitivity of the assay. The low allele frequency of the S-PATRR3 may also explain why only two PATRR3-related translocations have been reported to date. Similarly, the t(17;22) has not been detected in sperm from healthy individuals ($<5 \times 10^{-6}$) (37). From these results, we hypothesize that PATRR3 and PATRR17 are stable and less susceptible to translocation. Alternatively, spatial proximity

between PATRR3 and other relevant PATRR-containing chromosomes may not occur (50).

PATRR3 is located in or in proximity to FRA3B, in which frequent deletions and translocations are seen in various tumor cells (29,30,51). Therefore, we investigated the possibility of a relationship between PATRR3 instability and FRA3B deletions in normal human samples and in APH-treated human–mouse somatic cell hybrids. Many deletions were observed in proximity to FRA3B, but they did not include the PATRR3 region. Recurrent deletions were centered in intron 5 of the *FHIT* gene, which is approximately 600 kb away from PATRR3. From these results, we conclude that PATRR3 appears to be directly involved in PATRR3-related translocations, but not in the majority of FRA3B deletions. This finding suggests that PATRR instability may be limited to vulnerability to translocation and not enhanced susceptibility to deletion. In general, common fragile sites, such as FRA3B, are prone to breakage under certain culture conditions or as a result of treatment with specific agents (28). This instability has been thought to be sequence driven as a result of being prone to forming unusual secondary structures (52,53) and a paucity of activated replication origins in FRA3B following replication stress (54). Common fragile sites, including FRA3B, are composed of relatively AT-rich sequences (23,55). Therefore, they are likely to form unusual secondary DNA structures,,- which can impede DNA replication and induce genomic rearrangements (24,53). Despite the fact that PATRRs appear capable of forming hairpin secondary structures (Supplementary Figure 2), PATRR3 does not appear to be directly involved in the FRA3B deletions, at least in those we examined. This result corroborates a recent opinion that FRA3B fragility relies not on fork slowing or stalling caused by secondary structures, but on a paucity of replication initiation events in lymphoblast cell lines (54).

In conclusion, we have identified a PATRR on chromosome 3 that is involved in a recurrent palindrome-mediated translocation. In addition, the occurrence of de novo t(3;11)s and t(3;22)s in normal healthy male sperm indicate that PATRR-mediated translocations can also involve chromosome 3. This indicates that PATRR-mediated translocations are not unique to chromosome 22 but represent a universal pathway to chromosomal rearrangement. Analysis of chromosome 3p rearrangements shows that the PATRR3 sequence does not appear to be directly involved at the site of FRA3B deletions, suggesting a non-PATRR mechanism for fragile site instability. Thus, genomic rearrangements on 3p, in the PATRR and FRA3B regions, appear to have several different etiologies.

Data access numbers (GENBANK)

AB690558, AB690559, AB690560, AB690561, AB690562, AB690563, and AB690564.

Acknowledgment

The authors wish to thank Laura K. Conlin and Sharon E. Plon for providing technical assistance and invaluable reagents. These studies were supported by CA039926, from the National Cancer Institute (B.S.E.). The content is solely the responsibility of the authors and does not necessarily represent the official views of the National Cancer Institute or the National Institutes of Health. The studies were also supported by funds from the Charles E.H. Upham Chair in Pediatrics (B.S.E.). One of the authors, T.K., was supported by a JSPS Postdoctoral Fellowship for Research Abroad.

This manuscript is dedicated to the memory of Rosaline Willis (mother of B.S.E.). Her support and encouragement enabled the maturation of this research.

Supplementary data

Supplementary data related to this article can be found at http://dx.doi.org/10.1016/j.cancergen.2014.03.004.

References

1. Bacolla A, Wojciechowska M, Kosmider B, et al. The involvement of non-B DNA structures in gross chromosomal rearrangements. DNA Repair (Amst) 2006;5:1161–1170.
2. Wang G, Vasquez KM. Non-B DNA structure-induced genetic instability. Mutat Res 2006;598:103–119.
3. Zhao J, Bacolla A, Wang G, et al. Non-B DNA structure-induced genetic instability and evolution. Cell Mol Life Sci 2010;67:43–62.
4. Wells RD. Non-B DNA conformations, mutagenesis and disease. Trends Biochem Sci 2007;32:271–278.
5. Leach DR. Long DNA palindromes, cruciform structures, genetic instability and secondary structure repair. Bioessays 1994;16: 893–900.
6. Lewis SM, Cote AG. Palindromes and genomic stress fractures: bracing and repairing the damage. DNA Repair (Amst) 2006;5: 1146–1160.
7. Akgun E, Zahn J, Baumes S, et al. Palindrome resolution and recombination in the mammalian germ line. Mol Cell Biol 1997; 17:5559–5570.
8. Collick A, Drew J, Penberth J, et al. Instability of long inverted repeats within mouse transgenes. EMBO J 1996;15:1163–1171.
9. Gordenin DA, Lobachev KS, Degtyareva NP, et al. Inverted DNA repeats: a source of eukaryotic genomic instability. Mol Cell Biol 1993;13:5315–5322.
10. Edelmann L, Spiteri E, Koren K, et al. AT-rich palindromes mediate the constitutional t(11;22) translocation. Am J Hum Genet 2001;68:1–13.
11. Kurahashi H, Shaikh TH, Hu P, et al. Regions of genomic instability on 22q11 and 11q23 as the etiology for the recurrent constitutional t(11;22). Hum Mol Genet 2000;9:1665–1670.
12. Gotter AL, Nimmakayalu MA, Jalali GR, et al. A palindrome-driven complex rearrangement of 22q11.2 and 8q24.1 elucidated using novel technologies. Genome Res 2007;17:470–481.
13. Kehrer-Sawatzki H, Haussler J, Krone W, et al. The second case of a t(17;22) in a family with neurofibromatosis type 1: sequence analysis of the breakpoint regions. Hum Genet 1997;99: 237–247.
14. Kurahashi H, Shaikh T, Takata M, et al. The constitutional t(17; 22): another translocation mediated by palindromic AT-rich repeats. Am J Hum Genet 2003;72:733–738.
15. Sheridan MB, Kato T, Haldeman-Englert C, et al. A palindrome-mediated recurrent translocation with 3:1 meiotic nondisjunction: the t(8;22)(q24.13;q11.21). Am J Hum Genet 2010;87:209–218.
16. Gotter AL, Shaikh TH, Budarf ML, et al. A palindrome-mediated mechanism distinguishes translocations involving LCR-B of chromosome 22q11.2. Hum Mol Genet 2004;13:103–115.
17. Nimmakayalu MA, Gotter AL, Shaikh TH, et al. A novel sequence-based approach to localize translocation breakpoints identifies the molecular basis of a t(4;22). Hum Mol Genet 2003; 12:2817–2825.

18. Tan X, Anzick SL, Khan SG, et al. Chimeric Negative Regulation of p14ARF and TBX1 by a t(9;22) Translocation Associated with Melanoma, Deafness, and DNA Repair Deficiency. Hum Mutat 2013.
19. Kurahashi H, Inagaki H, Hosoba E, et al. Molecular cloning of a translocation breakpoint hotspot in 22q11. Genome Res 2007; 17:461–469.
20. Cohen AJ, Li FP, Berg S, et al. Hereditary renal-cell carcinoma associated with a chromosomal translocation. N Engl J Med 1979;301:592–595.
21. Poland KS, Azim M, Folsom M, et al. A constitutional balanced t(3;8)(p14;q24.1) translocation results in disruption of the TRC8 gene and predisposition to clear cell renal cell carcinoma. Genes Chromosomes Cancer 2007;46:805–812.
22. Gemmill RM, West JD, Boldog F, et al. The hereditary renal cell carcinoma 3;8 translocation fuses FHIT to a patched-related gene, TRC8. Proc Natl Acad Sci USA 1998;95:9572–9577.
23. Boldog F, Gemmill RM, West J, et al. Chromosome 3p14 homozygous deletions and sequence analysis of FRA3B. Hum Mol Genet 1997;6:193–203.
24. Mimori K, Druck T, Inoue H, et al. Cancer-specific chromosome alterations in the constitutive fragile region FRA3B. Proc Natl Acad Sci USA 1999;96:7456–7461.
25. Mulvihill DJ, Wang YH. Two breakpoint clusters at fragile site FRA3B form phased nucleosomes. Genome Res 2004;14:1350–1357.
26. Wilke CM, Guo SW, Hall BK, et al. Multicolor FISH mapping of YAC clones in 3p14 and identification of a YAC spanning both FRA3B and the t(3;8) associated with hereditary renal cell carcinoma. Genomics 1994;22:319–326.
27. Arlt MF, Durkin SG, Ragland RL, et al. Common fragile sites as targets for chromosome rearrangements. DNA Repair (Amst) 2006;5:1126–1135.
28. Durkin SG, Glover TW. Chromosome fragile sites. Annu Rev Genet 2007;41:169–192.
29. Durkin SG, Ragland RL, Arlt MF, et al. Replication stress induces tumor-like microdeletions in FHIT/FRA3B. Proc Natl Acad Sci USA 2008;105:246–251.
30. Glover TW, Coyle-Morris JF, Li FP, et al. Translocation t(3;8)(p14.2;q24.1) in renal cell carcinoma affects expression of the common fragile site at 3p14(FRA3B) in lymphocytes. Cancer Genet Cytogenet 1988;31:69–73.
31. Kurahashi H, Emanuel BS. Unexpectedly high rate of de novo constitutional t(11;22) translocations in sperm from normal males. Nat Genet 2001;29:139–140.
32. Kato T, Inagaki H, Yamada K, et al. Genetic variation affects de novo translocation frequency. Science 2006;311:971.
33. Gunderson KL, Steemers FJ, Lee G, et al. A genome-wide scalable SNP genotyping assay using microarray technology. Nat Genet 2005;37(5):549–554.
34. Zuker M. Mfold web server for nucleic acid folding and hybridization prediction. Nucleic Acids Res 2003;31:3406–3415.
35. Ohta M, Inoue H, Cotticelli MG, et al. The *FHIT* gene, spanning the chromosome 3p14.2 fragile site and renal carcinoma-associated t(3;8) breakpoint, is abnormal in digestive tract cancers. Cell 1996;84:587–597.
36. Kurahashi H, Shaikh TH, Zackai EH, et al. Tightly clustered 11q23 and 22q11 breakpoints permit PCR-based detection of the recurrent constitutional t(11;22). Am J Hum Genet 2000;67:763–768.
37. Inagaki H, Ohye T, Kogo H, et al. Palindromic AT-rich repeat in the *NF1* gene is hypervariable in humans and evolutionarily conserved in primates. Hum Mutat 2005;26:332–342.
38. Tong M, Kato T, Yamada K, et al. Polymorphisms of the 22q11.2 breakpoint region influence the frequency of de novo constitutional t(11;22)s in sperm. Hum Mol Genet 2010;19: 2630–2637.
39. Glover TW, Stein CK. Chromosome breakage and recombination at fragile sites. Am J Hum Genet 1988;43:265–273.
40. Kurahashi H, Inagaki H, Kato T, et al. Impaired DNA replication prompts deletions within palindromic sequences, but does not induce translocations in human cells. Hum Mol Genet 2009;18: 3397–3406.
41. Shaikh TH, Gai X, Perin JC, et al. High-resolution mapping and analysis of copy number variations in the human genome: a data resource for clinical and research applications. Genome Res 2009;19:1682–1690.
42. Kato T, Inagaki H, Kogo H, et al. Two different forms of palindrome resolution in the human genome: deletion or translocation. Hum Mol Genet 2008;17:1184–1191.
43. Kato T, Kurahashi H, Emanuel BS. Chromosomal translocations and palindromic AT-rich repeats. Curr Opin Genet Dev 2012;22: 221–228.
44. Bowater R, Aboul-ela F, Lilley DM. Large-scale stable opening of supercoiled DNA in response to temperature and supercoiling in (A + T)-rich regions that promote low-salt cruciform extrusion. Biochemistry 1991;30:11495–11506.
45. Dayn A, Malkhosyan S, Duzhy D, et al. Formation of (dA-dT)n cruciforms in Escherichia coli cells under different environmental conditions. J Bacteriol 1991;173:2658–2664.
46. Kato T, Inagaki H, Tong M, et al. DNA secondary structure is influenced by genetic variation and alters susceptibility to de novo translocation. Mol Cytogenet 2011;4:18.
47. Kurahashi H, Inagaki H, Ohye T, et al. Palindrome-mediated chromosomal translocations in humans. DNA Repair (Amst) 2006;5:1136–1145.
48. Tapia-Paez I, Kost-Alimova M, Hu P, et al. The position of t(11;22)(q23;q11) constitutional translocation breakpoint is conserved among its carriers. Hum Genet 2001;109:167–177.
49. Carter MT, St Pierre SA, Zackai EH, et al. Phenotypic delineation of Emanuel syndrome (supernumerary derivative 22 syndrome): clinical features of 63 individuals. Am J Med Genet A 2009;149A:1712–1721.
50. Ashley T, Gaeth AP, Inagaki H, et al. Meiotic recombination and spatial proximity in the etiology of the recurrent t(11;22). Am J Hum Genet 2006;79:524–538.
51. Fang JM, Arlt MF, Burgess AC, et al. Translocation breakpoints in FHIT and FRA3B in both homologs of chromosome 3 in an esophageal adenocarcinoma. Genes Chromosomes Cancer 2001;30:292–298.
52. Lukusa T, Fryns JP. Human chromosome fragility. Biochim Biophys Acta 2008;1779:3–16.
53. Mishmar D, Rahat A, Scherer SW, et al. Molecular characterization of a common fragile site (FRA7H) on human chromosome 7 by the cloning of a simian virus 40 integration site. Proc Natl Acad Sci USA 1998;95:8141–8146.
54. Letessier A, Millot GA, Koundrioukoff S, et al. Cell-type-specific replication initiation programs set fragility of the FRA3B fragile site. Nature 2011;470:120–123.
55. Shiraishi T, Druck T, Mimori K, et al. Sequence conservation at human and mouse orthologous common fragile regions, FRA3B/FHIT and Fra14A2/Fhit. Proc Natl Acad Sci USA 2001; 98:5722–5727.

PLOS ONE

Age-Related Decrease of Meiotic Cohesins in Human Oocytes

Makiko Tsutsumi[1], Reiko Fujiwara[1], Haruki Nishizawa[2], Mayuko Ito[1,2], Hiroshi Kogo[3], Hidehito Inagaki[1], Tamae Ohye[1], Takema Kato[1], Takuma Fujii[2], Hiroki Kurahashi[1]*

1 Division of Molecular Genetics, Institute for Comprehensive Medical Science, Fujita Health University, Toyoake, Aichi, Japan, **2** Department of Obstetrics and Gynecology, Fujita Health University, Toyoake, Aichi, Japan, **3** Department of Anatomy and Cell Biology, Gunma University Graduate School of Medicine, Maebashi, Gunma, Japan

Abstract

Aneuploidy in fetal chromosomes is one of the causes of pregnancy loss and of congenital birth defects. It is known that the frequency of oocyte aneuploidy increases with the human maternal age. Recent data have highlighted the contribution of cohesin complexes in the correct segregation of meiotic chromosomes. In mammalian oocytes, cohesion is established during the fetal stages and meiosis-specific cohesin subunits are not replenished after birth, raising the possibility that the long meiotic arrest of oocytes facilitates a deterioration of cohesion that leads to age-related increases in aneuploidy. We here examined the cohesin levels in dictyate oocytes from different age groups of humans and mice by immunofluorescence analyses of ovarian sections. The meiosis-specific cohesin subunits, REC8 and SMC1B, were found to be decreased in women aged 40 and over compared with those aged around 20 years ($P<0.01$). Age-related decreases in meiotic cohesins were also evident in mice. Interestingly, SMC1A, the mitotic counterpart of SMC1B, was substantially detectable in human oocytes, but little expressed in mice. Further, the amount of mitotic cohesins of mice slightly increased with age. These results suggest that, mitotic and meiotic cohesins may operate in a coordinated way to maintain cohesions over a sustained period in humans and that age-related decreases in meiotic cohesin subunits impair sister chromatid cohesion leading to increased segregation errors.

Citation: Tsutsumi M, Fujiwara R, Nishizawa H, Ito M, Kogo H, et al. (2014) Age-Related Decrease of Meiotic Cohesins in Human Oocytes. PLoS ONE 9(5): e96710. doi:10.1371/journal.pone.0096710

Editor: Qinghua Shi, University of Science and Technology of China, China

Received December 13, 2013; **Accepted** April 10, 2014; **Published** May 7, 2014

Funding: This work was supported by grants from JSPS KAKENHI (22790334 and 25860255 to MT and 21028020 and 23013019 to HK, URL: http://www.jsps.go.jp/j-grantsinaid/). The funders had no role in study design, data collection and analysis, decision to publish, or preparation of the manuscript.

Competing Interests: The authors have declared that no competing interests exist.

* E-mail: kura@fujita-hu.ac.jp

Introduction

Chromosomal segregation errors that arise during meiotic cell division produce aneuploid gametes with an incorrect number of chromosomes. Aneuploidy of fetal chromosomes causes miscarriage or results in newborns with congenital birth defects such as Down syndrome (DS). It is well known that the extra chromosome in trisomy 21 in DS mainly originates from segregation errors during maternal meiosis I, and that the risk of DS increases with maternal age [1,2]. The frequency of DS is 1/1400 births in 20–24 year-old women. This rises to 1/350 in 35-year-old and 1/25 in 45-year-old and older women [3]. In addition, age-related oocyte aneuploidy causes an elevated risk of pregnancy loss in older women i.e. the rate of chromosomal anomalies among clinically diagnosed miscarriages is about 50% in women younger than 35 but is 75% in women above this age. The incidence of miscarriage is 9% in women in their early 20 s and rises to 75% in women aged 45 and over [4,5]. These also indicate significant increase of aneuploidy in older women. However, the etiology of maternal age-related increases in chromosomal segregation errors remains unclear.

Meiotic cohesins have a key role in correct segregation of chromosomes in meiosis [6–8]. The ring-shaped cohesin complex is required for sister chromatid cohesion during meiosis and also in mitotic cell division. In mammalian oocytes, the establishment of cohesions during pre-meiotic DNA replication is followed by entry into prophase of meiosis I. After homologous chromosomes are connected at the crossover site via homologous recombination, the oocytes become arrested at the diplotene stage of prophase I for a prolonged period (dictyate stage) during the fetal stage. After sexual maturation, meiosis resumes and the first cell division occurs before ovulation. During this prolonged period, the homologous chromosomes are kept together until the onset of anaphase I by sister chromatid cohesion distal to the chiasma. However, it has been shown that SMC1B and REC8, meiosis-specific components of the cohesin complex, do not undergo turnover after birth in female mice [9,10]. It is possible that this might cause the gradual decrease in the cohesin levels. The deterioration of cohesion in the chromosome arm leads to meiosis I nondisjunction via the premature dissociation of chiasma between homologous chromosomes. This deterioration in the centromere induces predivision of sister chromatids. These events result increase the risk of age-related segregation error in humans [11–14].

To verify this hypothesis, the levels of the meiotic cohesin subunits, SMC1B and REC8, as well as the mitotic cohesin subunits, RAD21 and SMC1A, and the SMC3 subunit used in common between meiotic and mitotic cohesin complexes, was examined in dictyate oocytes from humans and mice. The immunofluorescence signal intensities on ovarian tissue sections

were quantified and demonstrated an age-related decrease in the meiosis-specific cohesins in both humans and mice. These results lend support to the hypothesis that a decrease in the cohesins with age induces chromosomal segregation errors. Moreover, these results highlight a novel hypothesis underlying the maintenance mechanism of cohesions in humans in which the life span is much longer than that of mice.

Materials and Methods

Ethics statement

This study was approved by the Ethical Review Board for Clinical Research at Fujita Health University. All of the patients gave written informed consent. All animal experiments were approved by the Animal Care and Use Committee at Fujita Health University (I0501).

Human ovarian tissue

Human ovarian tissues were obtained from 8 women (age range: 19–49 years) who were undergoing surgery for ovarian tumors at Fujita Health University Hospital. Samples were derived from the normal region within the dissected tumor. Ovarian tissues were immediately embedded in Tissue-Tek OCT compound (Sakura Finetek), snap-frozen in liquid nitrogen in the operating room and stored at −70°C within 1 hour of dissection.

Mice

C57BL/6NCr mice were obtained from Japan SLC. Ovaries from female mice were embedded, snap-frozen and stored at −70°C as described above.

Antibodies

Rabbit polyclonal anti-human REC8 antibodies were raised against amino acid residues 427–443 of the human REC8 protein. Rabbit polyclonal anti-human SMC1B antibodies were raised against amino acid residues 1219–1235 of the human SMC1B protein. Guinea pig polyclonal anti-mouse SMC1B antibodies were raised against amino acid residues 1215–1248 of mouse SMC1B. Guinea pig polyclonal anti-mouse REC8 antibodies were raised as described previously [15]. The resulting antisera were affinity purified on columns coupled to the peptide. The specificities of the antibodies described above were confirmed as shown in Figure S1. All antibodies used in this study are listed in Table S1.

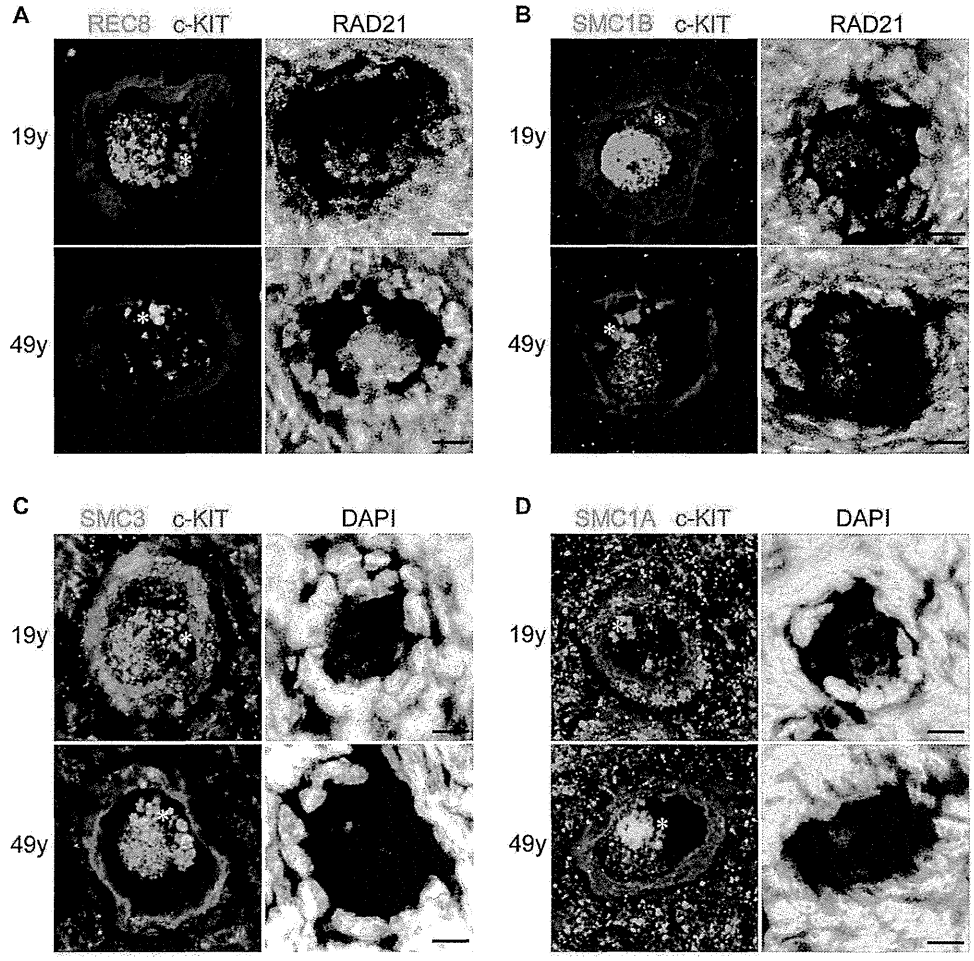

Figure 1. Immunofluorescent staining of human oocytes in ovarian sections from 19- and 49-year-old women. (A, B) REC8 or SMC1B (green) proteins co-immunostained with RAD21. (C, D) SMC3 or SMC1A (green) signals counterstained with DAPI. C-KIT (red) was used as a marker of oocytes. Asterisks indicate autofluorescence in the cytoplasmic region of the oocytes. Bar, 10 μm.
doi:10.1371/journal.pone.0096710.g001

Immunofluorescent staining

Ovarian frozen tissue sections were prepared and fixed as described previously [16]. Briefly, sections were fixed in methanol:acetone:chloroform (1:1:1) for 10 min on ice and then washed three times in PBS. After blocking with 10% normal donkey serum in PBS for 30 min at room temperature, staining with primary and secondary antibodies were performed as described [17]. The exception was when using biotin-conjugated secondary antibodies where the slides were incubated with Alexa Fluor 350-conjugaed streptavidin (Life Technologies) for 15 min and then washed three times after washing of the secondary antibodies.

Image analysis

Slides were observed under a fluorescence microscope (Axio Imager M1 or Axio Imager Z2, Carl Zeiss) equipped with a digital camera (AxioCam HRc, Carl Zeiss). Images were captured using the same settings controlled by Axiovision 4.8 software (Carl Zeiss). Densitometric analysis of the immunofluorescence signals from oocyte and somatic cell nuclei was performed using Axiovision 4.8 software. Schematic drawings explaining the method to determine the relative cohesin concentrations are described in Figure S2. Data analysis was performed using Excel software.

Results

Age-related decrease of meiosis-specific cohesins in human dictyate oocytes

To compare the cohesin levels in oocytes from women of different ages, we employed an immunofluorescence technique using ovarian tissue sections (Fig. 1). Cohesin complexes in oocytes consist of REC8, SMC1B and SMC3 subunits, whilst in somatic cells comprise RAD21, SMC1A and SMC3 subunits. By immunofluorescence staining, meiosis-specific cohesin subunits, REC8 and SMC1B, were detectable in the nuclei of dictyate oocytes and exhibited a threadlike distribution with dense aggregates as previously reported [18]. but not in somatic cells on ovarian tissue sections (Fig. 1A, B). SMC3, a shared cohesin subunit both meiotic and mitotic cells, could be detected in the nuclei of both oocytes and somatic cells (Fig. 1C). The mitotic cohesin subunits RAD21 and SMC1A, which are substituted in meiosis with meiosis-specific cohesins REC8 and SMC1B, respectively, were also detectable both in somatic cells and oocytes (Fig. 1A, B, D).

To determine the relative oocyte cohesin concentration, the immunofluorescent signals corresponding to mitotic cohesins in the nuclei of somatic cells were used to normalize the signal intensities among samples. REC8 or SMC1B proteins were immunostained along with RAD21 as an internal control

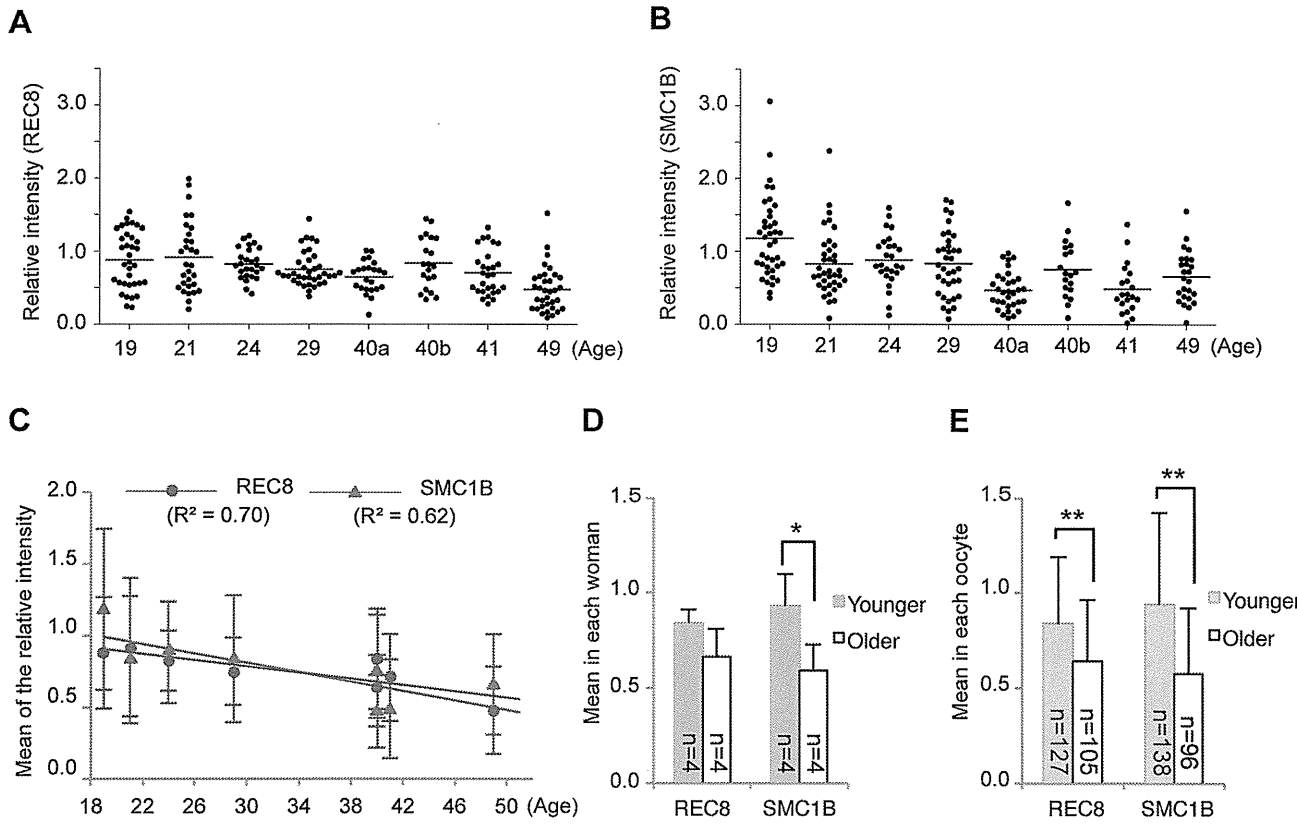

Figure 2. Quantitative results for meiosis-specific cohesins in human oocytes. (A, B) Relative signal intensity of REC8 or SMC1B. Intensities were determined as described in Figure S2. Specimens were obtained from two 40 year old female subjects (40a and 40b). Horizontal bars indicate the mean cohesin levels for each subject. (C) Regression analyses of the mean cohesin signal intensities shown in (A) and (B) (mean ± SD). The regression lines are indicated by solid lines. The coefficients of determination are indicated in parentheses. (D, E) Comparisons of the signal intensity means between grouped samples. Women were grouped as younger (≤29-year-old) or older (≥40-year-old). (D) The cohesin signal intensity means shown in (A–C) were compared between groups (mean ± SD). (E) The cohesin signal intensity means in single oocytes were compared between groups (mean ± SD). *$P<0.05$, **$P<0.01$, Student's *t*-test.
doi:10.1371/journal.pone.0096710.g002

(Fig. 1A, B). The relative amounts of cohesins in oocytes were estimated as a ratio of the signal intensity in oocytes to that of mitotic cohesins in somatic cells (Fig. S2).

We examined the signal intensity of meiosis-specific cohesins in oocytes from 8 women aged 19 to 49 years (Fig. 2A, B). Immunofluorescent signals for the meiosis-specific cohesins, REC8 and SMC1B, were detected in the oocytes of all samples examined (Fig. 1A, B). These signal intensities showed a wide distribution, which was partly due to the variability between each oocyte and also due to the position of the sections since the thicknesses of these sections are smaller than the diameter of the oocyte nuclei (Fig. 1A, B). We found that the mean REC8 and SMC1B signal intensities among individual women showed a negative correlation with age (Fig. 2C). We further analyzed these signal intensities by dividing our female subject into younger (≤29-year-old; mean ± SD: 23.3±4.3 year-old) and older (≥40-year-old; mean ± SD: 42.5±4.4 year-old) groups. The decrease observed in the SMC1B levels in the older group was significant although REC8 did not show a significant decrease (Fig. 2D). However, when the signal intensities of each oocyte were compared, the REC8 and SMC1B levels in the older group were significantly decreased by 24% and 38%, respectively, compared with the younger women (Fig. 2E). Similar results were obtained when REC8 was co-immunostained with pan-histone as another internal control (Fig. S3).

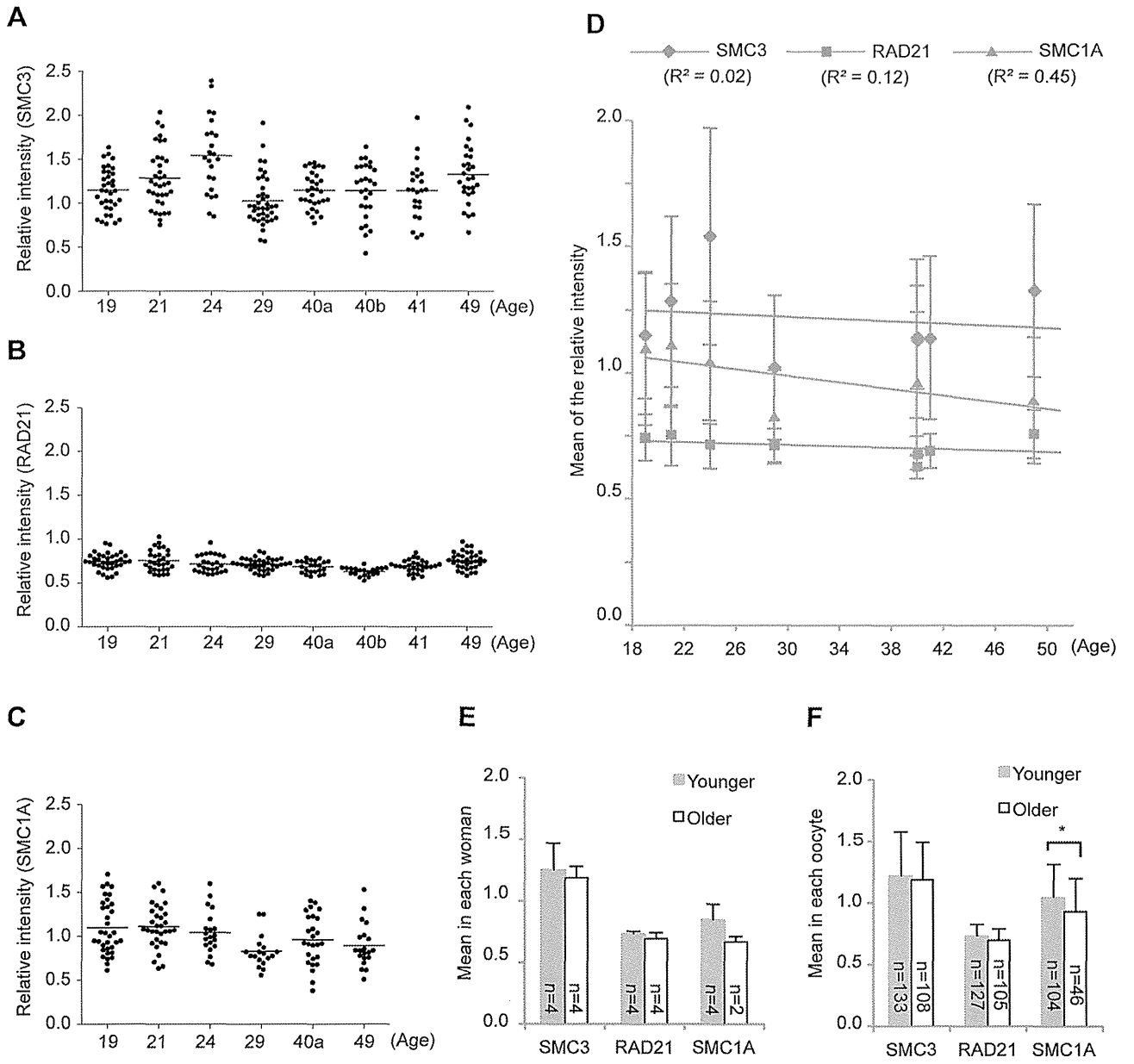

Figure 3. Quantitative results for the mitotic cohesin levels in human oocytes. (A–C) Relative signal intensities for SMC3, RAD21 or SMC1A. (D) Regression analyses of the cohesin signal intensity means shown in (A–C) (mean ± SD). Lines are the regression lines. The coefficients of determination are in parentheses. (E, F) Comparisons of the signal intensity means between grouped samples. Women were grouped as indicated in Figure 2. (E) The cohesin signal intensity means shown in (A–D) were compared between groups (mean ± SD). (F) The cohesin signal intensity means in single oocytes were compared between groups (mean ± SD). *$P<0.05$, Student's *t*-test.
doi:10.1371/journal.pone.0096710.g003